

## Magneto-Optical Kerr Effect in $\text{Nd}_2(\text{Mo}_{1-x}\text{Nb}_x)_2\text{O}_7$

S. Iguchi<sup>1</sup>, S. Kumakura<sup>1</sup>, Y. Onose<sup>1,2</sup> and Y. Tokura<sup>1,2,3</sup>

<sup>1</sup>Dept. of Applied Physics, Univ. of Tokyo, Tokyo 113-8656, Japan

<sup>2</sup>Multiferroics Project, ERATO, JST, Wako 351-0198, Japan

<sup>3</sup>Cross-Correlated Materials Research Group, ASI, RIKEN, Wako 351-0198, Japan

The origin of the anomalous Hall effect (AHE) has long been discussed since 1960's in terms of the band effect by Karplus-Luttinger, the spin fluctuation, and the side jump, etc. Recent theoretical studies on the AHE due to the Berry phase or the spin-chirality mechanism are the quantum theoretical extension from the traditional perturbative treatment by Karplus-Luttinger, and have revealed the significance of the resonant effect [1] at a small gap in band structure due to some kind of interaction, such as the spin-orbit interaction or the spin chirality.

Magneto-optical Kerr effect (MOKE) is an extension of AHE with respect to the energy range. The MOKE measurements for  $\text{Nd}_2\text{Mo}_2\text{O}_7$  with spin chirality and  $\text{Gd}_2\text{Mo}_2\text{O}_7$  without it have revealed that there is an enhancement in the mid-IR region of the off-diagonal optical conductivity  $\sigma_{xy}(\omega)$  originated from the spin chirality [2]. The scaling relation between the anomalous Hall conductivity and the longitudinal resistivity in  $\text{Nd}_2(\text{Mo}_{1-x}\text{Nb}_x)_2\text{O}_7$  (NMNO) with spin chirality [1] is in good agreement with the theoretical prediction, which should be considered as the resonant effect among the slightly gapped  $t_{2g}$  bands by the spin chirality. Thus, the direct observation of the resonant effect in  $\sigma_{xy}(\omega)$  is desired for the investigation on the origin of the AHE. The NMNO is suitable for the possible observation of the resonant structure in  $\sigma_{xy}(\omega)$  and its systematic change with the electron doping by  $\text{Nb}^{5+}$  (Fig. 1).

All the specimens used in this study were of single crystals synthesized by a floating-zone method. The reflectivity measurement has been performed from 20 meV to 40 eV for  $E||100$ . Especially for the energy range of 4-40eV, we used the spectrometer equipped

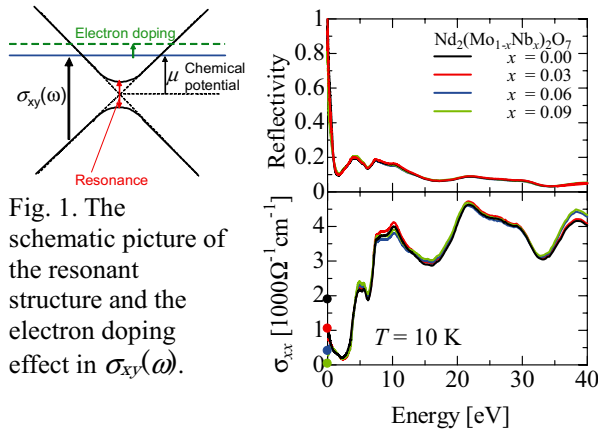


Fig. 2. The reflectivity and conductivity in NMNO. The temperature is 300 K for 4-40 eV range.

in BL-1B at UVSOR (see Fig. 2). Thus the highly accurate optical conductivity ( $\sigma_{xx}(\omega)$ ) was acquired. Then the  $\sigma_{xy}(\omega)$  was calculated with the obtained  $\sigma_{xx}(\omega)$  and the MOKE spectrum for the energy range of 0.1-4.5 eV.

Figure 3 shows the spectra of the optical conductivity, the real and imaginary components of  $\sigma_{xy}(\omega)$  in NMNO at 10 K. The  $\sigma_{xx}(\omega)$  shows the correspondent change with the dc conductivity (metallic to insulating with increasing  $x$ ) without remarkable anomaly such as a peak. In contrast, the characteristic peak structure was observed in the mid-IR range in the  $\sigma_{xy}(\omega)$  as well as the continuity to the dc value represented by the dots in the Fig. 2. Especially, some of the peak-top values are larger than dc ones meaning the resonance effect is intrinsic for the off diagonal conductivity. The shift of the peak to higher energy is considered as the increase in the chemical potential by Nb doping as depicted in Fig. 1.

In conclusion, we have demonstrated the resonance effect of bands in  $\sigma_{xy}(\omega)$ , which is in good accordance with the Berry phase theory, and revealed the  $\sigma_{xy}(\omega)$  is subject to the band structure.

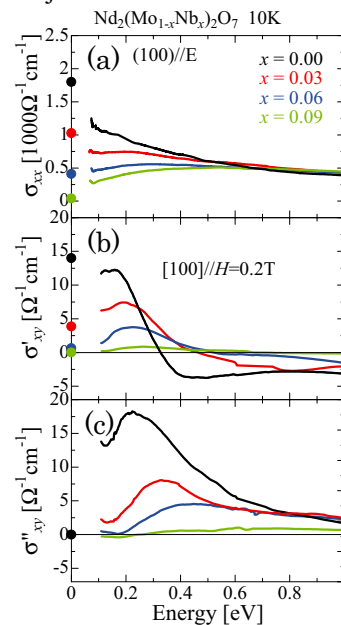


Fig. 3. (a) The optical conductivity, (b) the real and (c) the imaginary part of off-diagonal optical conductivity in NMNO at 10 K.

[1] S. Onoda *et al.*, Phys. Rev. B **77** (2008) 165103.

[2] I. Kézsmárki *et al.*, Phys. Rev. B **72** (2005) 094427.

[3] S. Iguchi *et al.*, Phys. Rev. Lett. **99** (2007) 077202.

## Investigation of Al K-Edge of Local Structure in Mesoporous Alumina Bulk with Fe Addition

A. Nakahira, T. Nishimoto, T. Kubo and T. Onoki

*Faculty of Engineering, Osaka Prefecture University, Gakuencho, Sakai 599-8531, Japan*

### Introduction

Much attentions have been paid to mesoporous materials. Among them, mesoporous alumina is also one of unique mesoporous materials because of their possible usages as a support material for catalysts and adsorption. However, the application of mesoporous alumina was restricted since mesoporous alumina was obtained only as a powder. The development of solidification of mesoporous alumina will expand the possibility of its application to various fields. After Nakahira et al reported that the dense bulk of zeolite was successfully synthesized using hydrothermal hot-pressing (HHP) method [1], it was found that the mesoporous materials could be also densified by hydrothermal hot-pressing (HHP) method. Here, we attempted to fabricate the dense bulks for mesoporous alumina containing with Fe salt. In this study, the local structure around Al of bulks of mesoporous alumina with Fe salt prepared by HHP method were investigated by XANES measurements.

### Experiments

Mesoporous alumina powder was synthesized as a starting material by a reference [2]. 2wt% Fe salt ( $\text{Fe}(\text{NO}_3)_2$ ) was added to mesoporous alumina powder, sufficiently mixed with alumina mortar and dried at 323 K. Mixture of these mesoporous alumina powders containing with Fe salt and water was heated at 110°C with uniaxial pressing under 40 MPa for 2 hours. Mesoporous alumina bulks obtained by hydrothermal hot-pressing (HHP) method were heat-treated at 723K in air atmosphere. Mesoporous alumina bulks were identified by XRD measurement.

Al K-edge XANES spectra for mesoporous alumina bulks were obtained in a total electron yield mode at room temperature using a KTP double-crystal monochromator at BL1A station of UVSOR. The spectra were collected in the photon energy range from 1520 to 1600 eV at intervals of 0.05 eV with a dwell time of 1 s.

### Results

Dense mesoporous alumina bulks containing with Fe salt were successfully obtained by hydrothermal hot-pressing (HHP) method and after heat-treatment at 723K in air atmosphere. XRD pattern of these showed that mesoporous alumina HHP bulk was also retained the mesoporous structure after HHP. Fe oxide as an additive was not detected by XRD for mesoporous alumina bulks containing with Fe salt obtained by hydrothermal hot-pressing (HHP) method. Figure 1 shows the results of Al K-edge XANES of

mesoporous alumina powder with Fe salt, HHP bulk from mesoporous alumina powder with Fe salt, and reference material powder ( $\alpha$ -alumina,  $\gamma$ -alumina, and  $\text{Al}(\text{OH})_3$ ). The spectrum of HHP bulk was significantly similar to those of starting powder and  $\gamma$ -alumina. Consequently, these results of XANES spectra revealed that the local structure around Al environment was almost unchanged before or after HHP treatment.

[1] A. Nakahira, S. Takezoe and Y. Yamasaki, *Chemistry Letters* **33** (2004) 1400.

[2] H. Nagata, M. Takimura, Y. Yamasaki and A. Nakahira, *Materials Transactions* **47** (2006) 2103.

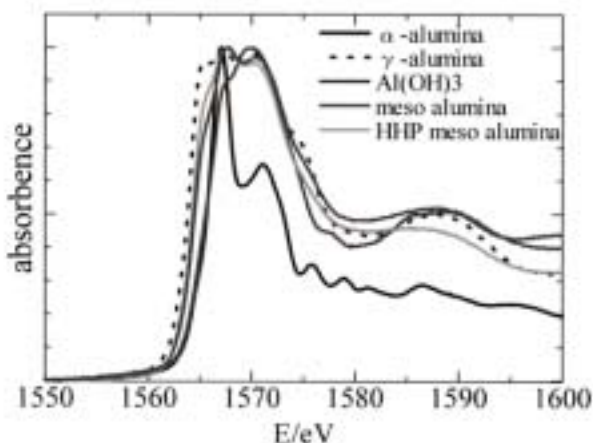


Fig. 1. Al K-edge XANES of mesoporous alumina powder with Fe salt, HHP bulk from mesoporous alumina powder with Fe salt, and reference material powder ( $\alpha$ -alumina,  $\gamma$ -alumina, and  $\text{Al}(\text{OH})_3$ ).

## Excitonic Structures of Reflection Spectra of $\text{Bi}_4\text{Ge}_3\text{O}_{12}$ and $\text{Bi}_{12}\text{GeO}_{20}$

T. Aoki<sup>1</sup>, H. Mitani<sup>1</sup>, T. Katagiri<sup>1</sup>, M. Itoh<sup>1</sup> and M. Fujita<sup>2</sup>

<sup>1</sup>*Dept. of Electrical and Electronic Engineering, Shinshu University, Nagano 380-8553, Japan*

<sup>2</sup>*Japan Coast Guard Academy, Kure 737-8512, Japan*

Bismuth germinate,  $\text{Bi}_4\text{Ge}_3\text{O}_{12}$ , and bismuth germanium oxide,  $\text{Bi}_{12}\text{GeO}_{20}$ , are usually abbreviated as BGO in common. The former (e-BGO) is a cubic crystal (space group  $I\bar{4}3d$ ) of the eulytine-type structure. The latter (s-BGO) is also cubic (space group  $I23$ ) with the sillenite-type structure. In the present experiment, the reflection spectra of e-BGO and s-BGO have been measured on the cleaved surfaces at  $T = 5$  and 300 K. Both crystals were obtained from Dr. Y. Usuki of Furukawa Co.

Figures 1(a) and 1(b) show the reflection spectra of e-BGO and s-BGO in a wide spectral range up to 35 eV at 5 K, respectively. The e-BGO exhibits a sharp lowest-energy peak at 4.81 eV followed by a weak peak at 5.15 eV, as clearly seen in Fig. 2(a). When  $T$  is increased from 5 to 300 K, the 4.81 and 5.15 eV bands are considerably broadened, the latter merging into the low-energy part of a broad band at around 6.25 eV. Such a feature reveals that these two bands are related to the excitonic transitions; i.e., the 4.81 and 5.15 eV bands are ascribed to the  $n = 1$  and  $n = 2$  excitons, respectively. The s-BGO exhibits a clear peak at 3.65 eV. This peak is also assigned to the excitonic  $6s \rightarrow 6p$  transition of  $\text{Bi}^{3+}$  ions. The  $n = 2$  exciton peak is not observed in s-BGO (Fig. 2(b)).

Assuming the simple hydrogen-like model of exciton, the energy of the  $n$ th level,  $E_n$ , is expressed as  $E_n = E_g - E_B/n^2$ , where  $E_g$  is the band-gap energy and  $E_B$  the exciton binding energy. By substituting the values of  $E_1$  and  $E_2$ , we obtain  $E_g = 5.26$  eV at 5 K and 5.17 eV at 300 K for e-BGO. Therefore, the value of  $E_B$  is estimated to be  $0.45 \pm 0.02$  eV at 5 and 300 K. On the other hand, the value of  $E_g$  in s-BGO is roughly determined to be 3.8 eV from the beginning of the rise of the reflectivity after the excitonic band, thus leading to  $E_B \approx 0.15$  eV.

The exciton binding energy is given by  $E_B = \mu e^4 / 2\hbar^2 \epsilon_\infty^2$ , where  $\mu$  is the reduced exciton mass,  $e$  the electron charge,  $\hbar$  the Planck constant, and  $\epsilon_\infty$  the optical dielectric constant. From  $\epsilon_\infty$  (e-BGO) = 4.67 and  $\epsilon_\infty$  (s-BGO) = 7.13, one can obtain  $\mu = 0.72m$  ( $m$ : free electron mass) for the exciton in e-BGO and  $\mu \approx 0.56m$  for s-BGO.

The reflection spectra above the band gap are briefly discussed by referring to our theoretical results calculated by the DV- $X\alpha$  method [1]. We ascribe the structures in the region of 5.5–12.5 eV in e-BGO and of 4.5–11.0 eV in s-BGO to the transitions from the valence band formed from the hybridized O 2p-Bi 6s states to the bottom of the conduction band. The structures in the region of 12.5–22.5 eV in e-BGO and of 11.5–22.0 eV in s-BGO are attributed to the transitions from the isolated Bi 6s state locating below the valence band to the entire conduction band.

Three peaks appearing in the 25–30 eV region in both BGOs are apparently due to the Bi 5d  $\rightarrow$  6p core exciton transitions.

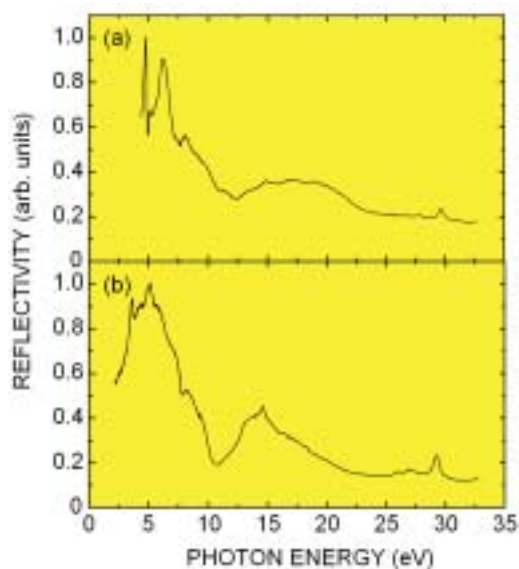
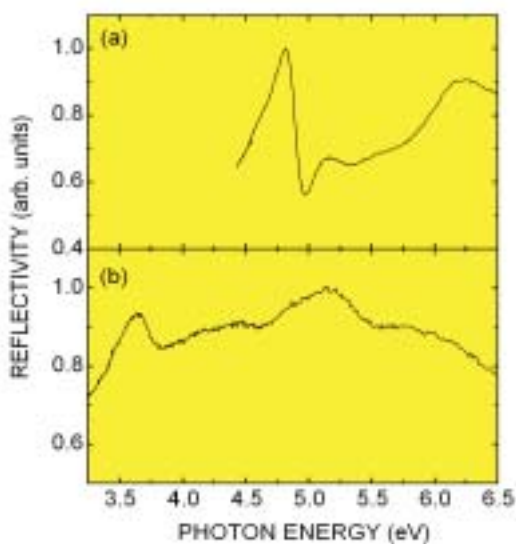


Fig. 1. Reflection spectra of (a) e-BGO and (b) s-BGO in a wide spectral range up to 35 eV measured at 5 K.

Fig. 2. Expanded spectra in the low-energy region of (a) e-BGO and (b) s-BGO shown in Fig. 1.



[1] M. Itoh, T. Katagiri, H. Mitani, M. Fujita and Y. Usuki, Phys. Status Solidi B **245** (2008) 2733.

## Polarization Dependence of Optical Transitions in CdMoO<sub>4</sub> and CdWO<sub>4</sub>

M. Fujita<sup>1</sup>, T. Katagiri<sup>2</sup>, D. Iri<sup>2</sup>, M. Itoh<sup>2</sup>, M. Kitaura<sup>3</sup> and V. B. Mikhailik<sup>4</sup>

<sup>1</sup>Japan Coast Guard Academy, Kure 737-8512, Japan

<sup>2</sup>Faculty of Engineering, Shinshu University, Nagano 380-8553, Japan

<sup>3</sup>Fukui National College of Technology, Sabae 916-8507, Japan

<sup>4</sup>Physics Department, University of Oxford, Oxford OXI 3RH, United Kingdom

Metal tungstates and molybdates are widely used as scintillating detectors in high-energy particle physics, rare event searches, and medical diagnoses. It is interesting to compare the optical spectra of CdMoO<sub>4</sub> with those of CdWO<sub>4</sub>, since the former crystallizes in the scheelite structure and the latter in the wolframite structure. In CdMoO<sub>4</sub> crystal, each Mo site is surrounded by four equivalent O sites to form MoO<sub>4</sub><sup>2-</sup> molecule of approximately tetrahedral symmetry. In CdWO<sub>4</sub> crystal, each W site is surrounded by six O sites in approximately octahedral symmetry. The WO<sub>6</sub><sup>6-</sup> octahedra form a chain by edge sharing. In the present study, the optical spectra of CdMoO<sub>4</sub> and CdWO<sub>4</sub> have been investigated in order to clarify their electronic structures.

Reflectivity spectra were measured at 10 K for oriented single crystals of CdMoO<sub>4</sub> and CdWO<sub>4</sub> using the polarized light parallel to the a-axis (**E**//**a**) and c-axis (**E**//**c**). The real ( $\epsilon_1$ ) and imaginary ( $\epsilon_2$ ) parts of the dielectric functions were calculated from the reflectivity spectra using a Kramers-Kronig analysis.

Figures 1(a) and 1(b) show the  $\epsilon_2$  spectra of CdMoO<sub>4</sub> and CdWO<sub>4</sub>, respectively. It appears that there is no obvious similarity in the  $\epsilon_2$  spectra between CdMoO<sub>4</sub> and CdWO<sub>4</sub>. The valence bands of both materials consist of the O 2*p* state. The conduction band is mainly made of the Mo 4*d* or W 5*d* states. The lower and upper parts of the conduction band are associated with the *e* and *t*<sub>2</sub> states, respectively, in the scheelite crystals, and vice versa in the wolframite crystals, due to the crystal-field splitting of the *d* state. The structures in regions I and II of CdMoO<sub>4</sub> in Fig. 1(a) are assigned to the transitions to the lower part of the conduction band with the *e* character and to the upper part with the *t*<sub>2</sub> character, respectively. As for CdWO<sub>4</sub>, the structures in regions I and II in Fig. 1(b) are ascribed to the transitions to the lower *t*<sub>2</sub> state and to the upper *e* state, respectively.

According to theoretical calculations by the DV- $X\alpha$  method [1, 2], the Cd 5*s* state significantly contributes to the bottom of the conduction band in both materials. For scheelite CdMoO<sub>4</sub>, we propose an energy-level diagram shown in Fig. 2. In a free MoO<sub>4</sub><sup>2-</sup> molecule of *T*<sub>d</sub> symmetry, the highest occupied orbital made of the O 2*p* state is of *t*<sub>1</sub> symmetry, while the lowest unoccupied orbital made of the Mo 4*d* state is of *e* symmetry. In the scheelite crystal they split into sublevels, because the site symmetry of the MoO<sub>4</sub><sup>2-</sup> molecule is lowered to *S*<sub>4</sub>. The Cd 5*s* state forms an energy level, which couples with a sublevel of the

same symmetry originating from the Mo 4*d* state. The dichroism in region I in Fig. 1(a) can be explained in terms of the assignment in Fig. 2.

In wolframite CdWO<sub>4</sub>, the WO<sub>6</sub><sup>6-</sup> octahedra form chains along the *c* axis. It is supposed that the intensity of the transition from the O site in the chain to the Cd site outside of the chain highly depends on the direction of the polarization with respect to the chain axis. Then the structures exhibiting the dichroism on the broad band in region I in Fig. 1(b) are attributed to the transitions to the Cd 5*s* state, which hybridizes with the W 5*d* conduction state.

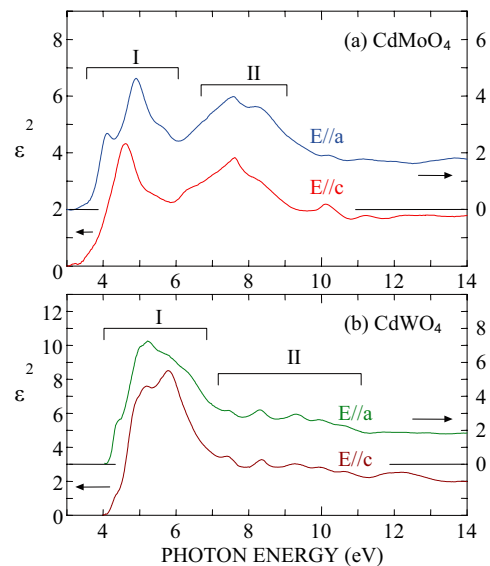


Fig. 1. Imaginary parts of the dielectric functions of (a) CdMoO<sub>4</sub> and (b) CdWO<sub>4</sub> for **E**//**a** and **E**//**c** at 10K.

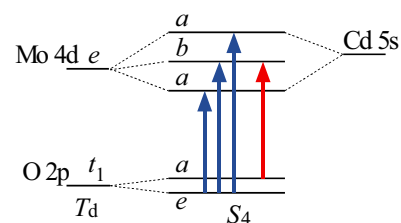


Fig. 2. Schematic diagram of the energy levels of CdMoO<sub>4</sub>. Blue and red arrows indicate the optical transitions allowed for **E**//**a** and **E**//**c**, respectively.

[1] M. Itoh, N. Fujita and Y. Inabe, J. Phys. Soc. Jpn. **75** (2006) 084705.

[2] M. Fujita *et al.*, Phys. Rev. B **77** (2008) 155118.

## Effect of Crystallization on the Photoluminescence in LaAlO<sub>3</sub> Induced by Ultraviolet Photons

T. Iikura, E. Hirata and Y. Ohki

Dept. Electrical Engineering and Bioscience, Waseda University, Shinjuku 169-8555, Japan

Lanthanum aluminate (LaAlO<sub>3</sub>) has been attracting much attention as a promising candidate for a gate insulator in advanced metal-oxide-semiconductor devices. In order to analyze its photoluminescence (PL) properties, we have been measuring PL and PL excitation (PLE) spectra for amorphous and crystalline LaAlO<sub>3</sub>.

### Experimental

The samples examined are LaAlO<sub>3</sub> (100) single crystals grown by the Czochralski method and LaAlO<sub>3</sub> thin films prepared by a spin-coating method. The films were annealed in oxygen at designated temperatures between 600 and 1000 °C. Using synchrotron radiation under multibunch operation at the BL1B line of UVSOR Facility as a photon source, PL, PLE, and absorption spectra were measured at 10 K. Crystallization of thin films was confirmed by in-plane X-ray diffraction (XRD) measurements.

### Results and Discussion

Figure 1 shows PL spectra of LaAlO<sub>3</sub> excited at 5.1 and 6.4 eV. Although the films annealed at 600 and 700 °C have no PL peaks, those annealed at 800, 900, and 1000 °C and the single crystal have three sharp PL peaks at around 1.60, 1.65, and 1.68 eV. The PL excited at 6.4 eV is much more intense than the one excited at 5.1 eV. Figure 2 shows PLE spectra measured for the three PLs. Note that each PLE spectrum is normalized to each maximum intensity. For all the samples, the PLE spectrum starts to rise at around 5.7 eV.

As shown in Fig. 3, both the single crystal and the film annealed at 900 °C show a sharp increase in absorption at 5.7 eV, while the film annealed at 600 °C shows a similar increase at 6.2 eV. The two energies agree with the band-gap energies of LaAlO<sub>3</sub> reported for its crystalline and amorphous states [1]. Furthermore, 5.7 eV corresponds to the energy at which the PLE spectra detected at 1.60, 1.65, and 1.68 eV show an abrupt increase in Fig. 2. From these results, the three PLs at around 1.60, 1.65, and 1.68 eV are assumed to be caused by de-excitation of electrons excited to the conduction band.

The XRD patterns shown in Fig.4 indicate the formation of a perovskite structure in the films if they are annealed at 800 °C or higher. Namely, the three sharp PL peaks around 1.60, 1.65, and 1.68 eV appear only in crystalline LaAlO<sub>3</sub>. The luminescence due to Cr<sup>3+</sup> in Al<sub>2</sub>O<sub>3</sub> has been reported to appear only when the sample is crystalline, and the mechanism underlying this is that the corresponding spin-forbidden transition in Cr<sup>3+</sup> becomes possible owing to spin-orbit mixing induced by the crystal field [2,3]. Taking these facts into consideration, the

three PLs in LaAlO<sub>3</sub> are assumed to be due to impurities.

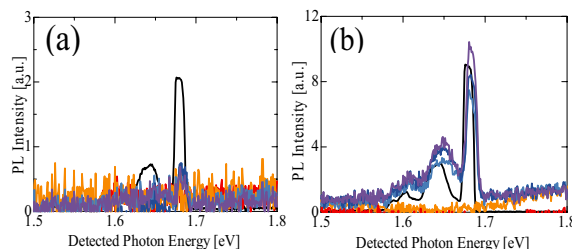


Fig. 1. PL spectra at 10 K induced by 5.1 eV photons (a) and by 6.4 eV photons (b) observed in LaAlO<sub>3</sub> films annealed at 600 °C (—), 700 °C (—), 800 °C (—), 900 °C (—), and 1000 °C (—), and similarly obtained PL spectra of single crystal LaAlO<sub>3</sub> (—). The numerals on the vertical axes should be multiplied by 10 only for the PL intensity of the single crystal (—).

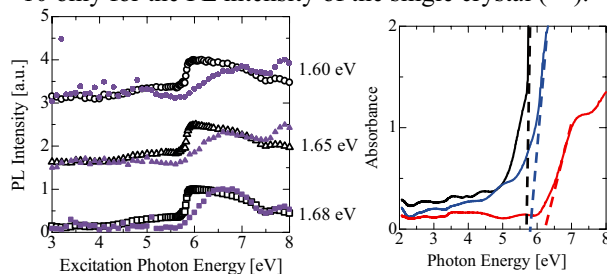


Fig. 2. PL intensities at 10 K detected at 1.60, 1.64, and 1.68 eV, induced in LaAlO<sub>3</sub> by photons with various energies. Solid symbols are for the film annealed at 1000 °C (●, ▲, ■), while open symbols are for the single crystal (○, △, □).

Fig. 3. Absorption spectra observed for LaAlO<sub>3</sub> films annealed at 600 °C (—) and 900 °C (—), and for single crystal (—).

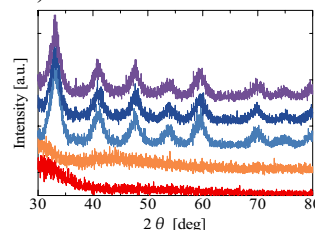


Fig. 4. XRD patterns of the LaAlO<sub>3</sub> films annealed at 600 °C (—), 700 °C (—), 800 °C (—), 900 °C (—), and 1000 °C (—).

- [1] L. F. Edge *et al.*, Appl. Phys. Lett. **84** (2004) 726.
- [2] J. Kákoš and L. Baca, J. Sol-gel Sci. Technol. **21** (2001) 167.
- [3] G. Carturan *et al.*, J. Matr. Sci. **25** (1990) 2705.

## Luminescence Properties of Undoped and N-Doped TiO<sub>2</sub> Powders Prepared by a Conventional Sol-Gel Method

T. Kawai<sup>1</sup>, Y. Kishimoto<sup>1</sup> and K. Kifune<sup>1,2</sup>

<sup>1</sup>*Department of Physical Science, Graduate School of Science, Osaka Prefecture University, Osaka 599-8531, Japan*

<sup>2</sup>*Faculty of Liberal Arts and Sciences, Osaka Prefecture University, Osaka 599-8531, Japan*

Recently, R. Asahi *et al.* reported that substitutional doping of nitrogen into TiO<sub>2</sub> contributed to narrowing of the band gap, thus providing a visible-light response [1]. According to other groups' studies, though the nitrogen doping induces new optical absorption bands in the visible-light region, absorbance is not linearly proportional to the photocatalytic activity [2]. The contribution of the nitrogen doping may be revealed by luminescence properties, because photoluminescence (PL) and excitation (PLE) spectra have been widely used to investigate the trapping, migration, and relaxation of the photo-excited carriers. In this study, we measure the PL and PLE spectra of undoped and N-doped TiO<sub>2</sub> powder specimens at the BL-1B line of UVSOR.

Undoped TiO<sub>2</sub> powders were prepared by a conventional sol-gel method. The TiO<sub>2</sub> powders obtained were annealed for 1 h in air at 500 °C in order to transform into anatase phase. N-doped TiO<sub>2</sub> powders were obtained by sintering the anatase TiO<sub>2</sub> powders together with urea at 500 °C.

Figure 1 shows the PL spectra of the undoped and N-doped TiO<sub>2</sub> powder specimens at 10 K. The broad luminescence bands around 2.23 and 2.63 eV are observed for the undoped and N-doped TiO<sub>2</sub> powders, respectively. In the undoped TiO<sub>2</sub> specimen, the luminescence bands exhibit the Gaussian-like band shape. On the other hand, the luminescence bands of the N-doped TiO<sub>2</sub> specimen have the shoulder structures at 2.46 and 2.83 eV and the lower energy tail. The difference of the peak energy and band shape between both the specimens implies that of the origin of the luminescence. The origin of the luminescence band in anatase TiO<sub>2</sub> is considered to be self-trapped excitons, excitons or electrons trapped around oxygen defects [3]. Many studies on N-doped TiO<sub>2</sub> demonstrate that N-related levels are formed above the valence band composing of oxygen 2p states [2, 4]. Therefore, the luminescence bands in the N-doped TiO<sub>2</sub> powder would be attributed to the radiative recombination of the electron with holes bound to the N-related levels.

Figure 2 shows the PLE spectra for the luminescence of the undoped and N-doped TiO<sub>2</sub> powder specimens at 10K. In the undoped TiO<sub>2</sub> powder, the PLE spectrum exhibits the response rising sharply from 3.32 eV, reflecting the band gap of anatase TiO<sub>2</sub>. On the other hand, the PLE spectrum for the 2.64 eV luminescence of the N-doped TiO<sub>2</sub> powder has the rise

from 2.83 eV and the step-like shoulder at 3.23 eV. The energy position of the step-like shoulder is close to the band gap energy of anatase TiO<sub>2</sub>. Thus, the response below 3.23 eV would be attributed to the nitrogen doping, that is to say, the transitions from the N-related levels to the conduction band. In order to clarify the contribution of nitrogen doping, the further studies on the luminescence properties are needed for TiO<sub>2</sub> with various amount of doped nitrogen.

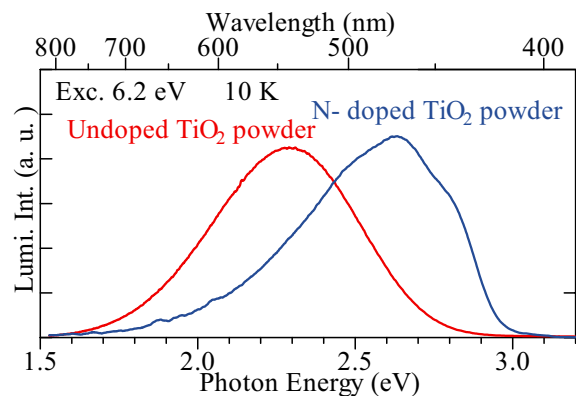


Fig. 1. PL spectra of undoped (red) and N-doped (blue) TiO<sub>2</sub> powder specimens at 10K.

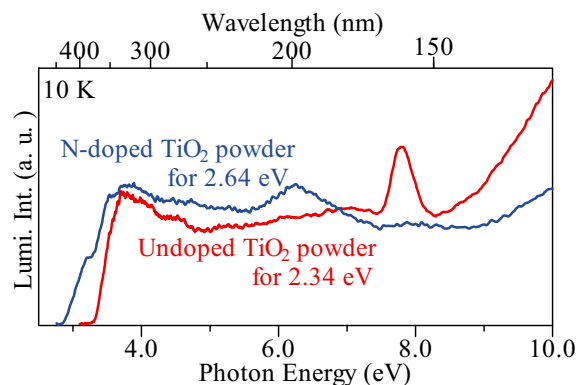


Fig. 2. PLE spectra of undoped (red) and N-doped (blue) TiO<sub>2</sub> powder specimens at 10 K.

- [1] R. Asahi *et al.*, *Science* **293** (2001) 269.
- [2] R. Nakamura *et al.*, *J. Phys. Chem. B* **108** (2004) 10617.
- [3] S. Mochizuki *et al.*, *Physica B* **340-342** (2003) 956.
- [4] C. D. Valentin *et al.*, *Chem. Phys.* **339** (2007) 44.

## Secondary Excitation Process by Hot Photocarriers in Inorganic EL Phosphors

M. Kitaura<sup>1</sup>, H. Mitani<sup>2</sup> and M. Itoh<sup>2</sup>

<sup>1</sup>*Fukui National College of Technology, Sabae 916-8507, Japan*

<sup>2</sup>*Department of Electrical and Electronics Engineering, Shinshu University, Nagano 380-8553, Japan*

In general, it is known that electroluminescence (EL) of inorganic phosphors is caused by the impact excitation of valence electrons by hot electrons; hot electron excitation. On the other hand, hot hole excitation has been found to occur in narrow-gap semiconductors, but there is no report on it in EL phosphors. Recently, Tanaka and Okamoto have reported that the hot hole excitation predominantly takes place in single insulating EL devices with SrGa<sub>2</sub>S<sub>4</sub>:Eu<sup>2+</sup> thin film [1]. Similar phenomena are also found in EuGa<sub>2</sub>S<sub>4</sub> [2] and BaAl<sub>2</sub>S<sub>4</sub>:Eu<sup>2+</sup> [3]. In contrast, they claim that hot electrons play a predominant role for the impact excitation in SrGa<sub>2</sub>S<sub>4</sub>:Ce<sup>3+</sup> thin film [1].

The aim of the present study is to inspect the above mentioned difference on hot carrier type between SrGa<sub>2</sub>S<sub>4</sub>:Eu<sup>2+</sup> and SrGa<sub>2</sub>S<sub>4</sub>:Ce<sup>3+</sup> phosphors. These phosphors show the green emission around 536 nm and the blue emission around 445 nm, respectively, under excitation with uv photons. We have measured photoluminescence excitation (PLE) spectra for the green and blue emission at 300 K, in order to investigate the lowest energy excitation process due to the creation of hot photocarriers. For better understanding of the structures in PLE spectra, we have also calculated the energy level structure of SrGa<sub>2</sub>S<sub>4</sub> by using the relativistic DV-X $\alpha$  method [4].

Figures 1(a) and 1(b) show the PL and PLE spectra of SrGa<sub>2</sub>S<sub>4</sub>:Eu<sup>2+</sup> and SrGa<sub>2</sub>S<sub>4</sub>:Ce<sup>3+</sup>, respectively. Both spectra were corrected for the spectral distribution of excitation light by using the sodium salicylate phosphor. The PL spectrum is also shown in each figure by a red line. As seen in both PLE spectra, the PL intensity is large below 4.4 eV, where the 4f $\rightarrow$ 5d absorption occurs efficiently. As the photon energy increased, the PL intensity is rapidly decreased at 4.4 eV, the energy of which is in good agreement with the fundamental absorption edge energy of SrGa<sub>2</sub>S<sub>4</sub>, determined from an analysis of the transmittance spectrum. Further increase in photon energy leads to the PL enhancement around 10 eV. This feature is interpreted as an indication of hot carrier excitation, because the hot carriers can gain the energy enough to excite valence electrons by the interband Auger mechanism.

In our calculation, the energy gap  $E_g$  and the valence band width  $E_{VB}$  were determined to be 4.57 eV and 6.56 eV, respectively. The value of  $E_{VB}$  is larger than that of  $E_g$ , and thus the condition for hot hole excitation  $E_{VB} > E_g$  is satisfied in host SrGa<sub>2</sub>S<sub>4</sub>. However, since the optical transition from the valence

band (VB) to the upper conduction band (CB) is expected to predominantly occurs in the 11-21 eV region, the hot hole excitation should be negligibly small even if it happens. Therefore, it is more likely that the PL enhancement around 10 eV is caused by hot photoelectron excitation.

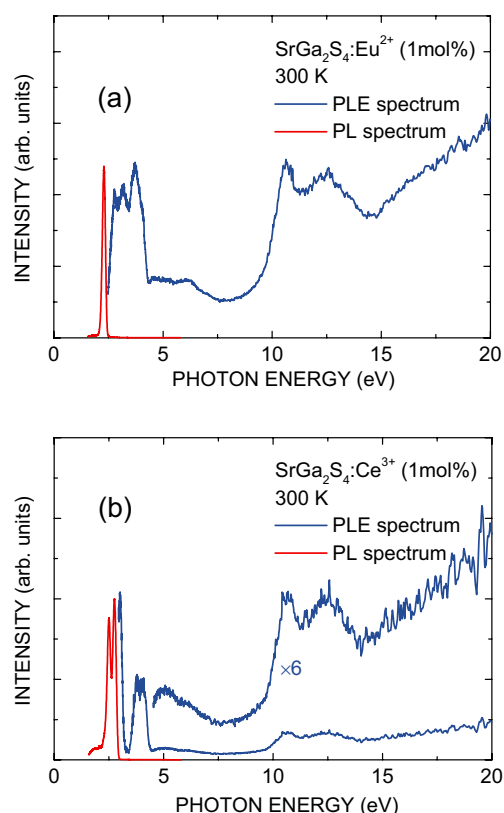


Fig. 1. Photoluminescence excitation (PLE) spectra of SrGa<sub>2</sub>S<sub>4</sub>:Eu<sup>2+</sup> (a) and SrGa<sub>2</sub>S<sub>4</sub>:Ce<sup>3+</sup> (b) phosphors. Both spectra were measured at 300 K. The PL spectra are also shown in the figures.

- [1] K. Tanaka and S. Okamoto, Appl. Phys. Lett. **89** (2006) 203508.
- [2] K. Tanaka and S. Okamoto, Appl. Phys. Lett. **83** (2003) 647.
- [3] K. Tanaka and S. Okamoto, Proc. of IDW'06 (2006) 1207.
- [4] H. Adachi, M. Tsukada and C. Satoko, J. Phys. Soc. Jpn. **45** (1978) 875.

## Photoluminescence of Hydroxyapatite Irradiated by Ultraviolet Synchrotron Orbital Radiation Light (5)

M. Ohta

*Department of Material Science and Technology, Faculty of Engineering, Niigata University, Niigata 950-2181, Japan*

It was known that rare earth ions dosed for oral administration to mouse and rat are transferred to blood vessel through the ileum and deposited its teeth and bone, which mainly consists of hydroxyapatite ( $\text{Ca}_{10}(\text{PO}_4)_6(\text{OH})_2$ ) [1-2]. Recently, rare earth is also useful as a contrast medium for magnetic resonance imaging, restriction enzyme, biocatalyst, and so on in fields of biochemistry, physiology, medicine, etc. However, the behavior of rare earth in the living body system remains an open question until now. We have found that Eu ion substituted Ba ion in Eu doped  $\text{Ba}_{10}(\text{PO}_4)_6\text{Cl}_2$  phosphor, which matrix is apatite structure [3]. The Eu ions, Gd ions or Yb ions are also found to substitute easily for calcium ions in hydroxyapatite which is soaked in  $\text{EuCl}_3$ ,  $\text{GdCl}_3$  or  $\text{YbCl}_3$  aqueous solution, and to play on emission center.

In this study, hydroxyapatite samples doped with  $\text{SmCl}_3$  aqueous solution were prepared in order to apply to phosphor. Their characteristics were investigated by photoluminescent property of Sm ion-doped hydroxyapatite samples excited by ultraviolet synchrotron orbital radiation light.

Sm-doped hydroxyapatite samples were prepared as follows: hydroxyapatite was soaked in  $\text{SmCl}_3$  aqueous solution. After 72 hr, Sm doped

hydroxyapatite was separated from  $\text{SmCl}_3$  aqueous solution by filtration and then dried by using with infrared ray.

The photoluminescent property of each sample excited by ultraviolet synchrotron orbital radiation light (BL1B) was observed by using with a multi-channel analyzer.

Figure 1 shows photoluminescence spectra of Sm ion-doped hydroxyapatite samples excited by BL-1B. The photoluminescence spectra of fired sample have the peak due to  $^4\text{G}_{5/2} \rightarrow ^6\text{H}_{5/2}$  (570nm),  $^4\text{G}_{5/2} \rightarrow ^6\text{H}_{7/2}$  (606nm),  $^4\text{G}_{5/2} \rightarrow ^6\text{H}_{9/2}$  (652nm) and  $^4\text{G}_{5/2} \rightarrow ^6\text{H}_{11/2}$  (713 nm), regardless of excitation wave length from 100 to 240 nm. The peak intensity is higher at 160 and 190 nm of excitation wave length. The peak intensity decreases with the wave length form 100nm to 130nm. This phenomenon is thought to be due to the multi-electron excitation.

[1] S. Hirano and K. T. Suzuki, Environ. Health Perspect. **104** (Supplement 1) (1996) 85.

[2] K. Kostial, B. Kargacin and M. Lendeka, Int. J. Radiat. Biol. Relat. Stud. Phys. Chem. Med. **51** (1987) 139.

[3] M. Sato, T. Tanaka and M. Ohta, J. Electrochem. Soc. **141** (1994) 1851.

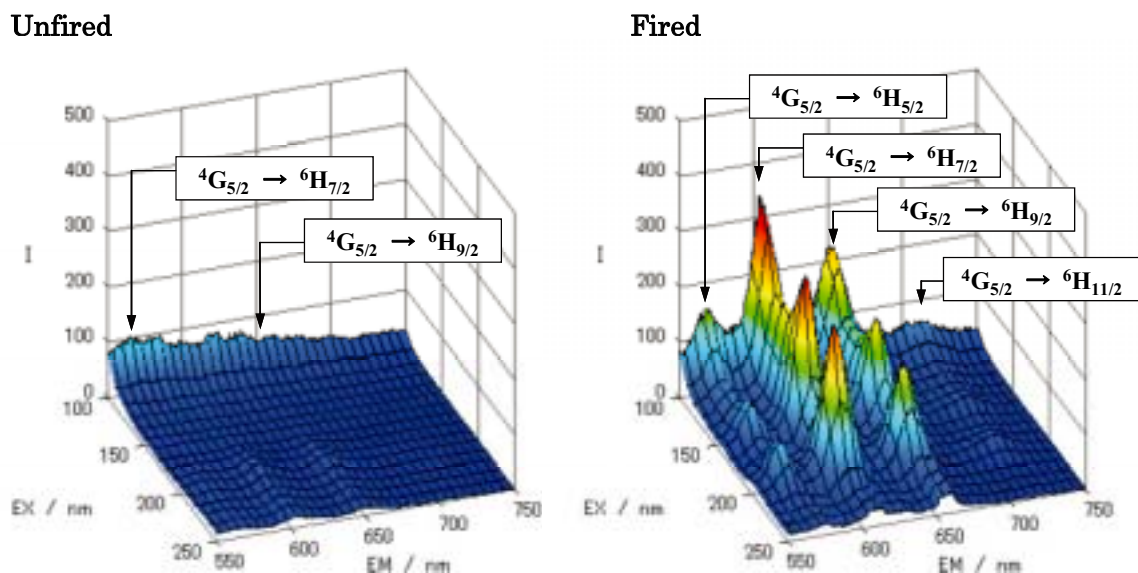


Fig. 1. Photoluminescent spectra of Sm ion-doped hydroxyapatite samples excited by ultraviolet synchrotron orbital radiation light.

# Local Electronic Structure Near the Energy Gap of Organic Solids Studied by X-Ray Emission Spectroscopy: The Case of Phthalocyanines

H. Yamane<sup>1</sup>, T. Hatsui<sup>2</sup> and N. Kosugi<sup>1</sup>

<sup>1</sup>*Institute for Molecular Science, Okazaki 444-8585, Japan*

<sup>2</sup>*XFEL Project Head Office, RIKEN and PRESTO, JST, Sayo-gun, Hyogo 679-5148, Japan*

## Introduction

Photon-in-photon-out techniques using synchrotron radiation such as fluorescence-yield X-ray absorption spectroscopy (FY-XAS) and X-ray emission spectroscopy (XES) measure the intensity distribution of emitted X-rays by the decay process of an inner-shell excitation, which gives unoccupied and occupied partial density-of-states of non-ionized or ionized materials. In these techniques, problems encountered with usual electron spectroscopies, such as charging, sample atmosphere, or disturbance from electric/magnetic fields, are negligible. The FY-XAS and XES are therefore powerful techniques for studies of large energy-gap materials and electric/magnetic-field-applied materials. Furthermore, the attenuation length of photons in the soft X-ray region is typically tens or hundreds of nanometers, which realizes an inherent bulk-sensitive method. In addition, such bulk sensitivity makes it possible to study buried interfaces of functional materials covered by different materials such as metal electrodes [1].

In this study, in order to understand the local electronic structure of organic semiconductors in the bulk phase, which is in principle difficult to study just by using the conventional ultraviolet photoemission spectroscopy (UPS) due to the charging problem of the sample, we have performed the FY-XAS and XES experiments on various metal-phthalocyanine (M-Pc; M = Zn, Cu, Mn, and H<sub>2</sub>) crystalline films.

## Experimental

The purified M-Pc materials were deposited onto the SiO<sub>2</sub>/Si(111) surface at room temperature. The deposited 200-nm-thick films show clear polar-angle dependence in the FY-XAS spectra (not shown), indicating a good crystallinity of the film. All the crystalline films were introduced to the spectrometer chamber at BL3U. The XES spectra were obtained by using a transmission-grating spectrometer [2]. Since the combination between a small photon-beam spot of 20 μm (vertical) × 40 μm (horizontal) with a photon flux of 10<sup>11</sup> ph/sec and an exposure time of 40–60 min induces significant radiation damage in organic solids, samples were translated at a rate of 20 μm/min during the XES measurements. Judging from the observed XES spectra, no oxygen-related contamination (see, Fig. 1 left panel) and no damage-induced defects exist in the present samples.

## Results and Discussion

The right panel in Fig. 1 shows the comparison of the C Kα and N Kα normal XES (NXES) spectra of the ZnPc crystalline film ( $h\nu_i = 295$  eV and 420 eV for C Kα and N Kα, respectively) with an UPS spectrum of a 10-nm-thick ZnPc thin film ( $h\nu_i = 40$  eV). The relative energies of the transition peaks in NXES correspond well with those of the valence-level peaks in UPS, except for the topmost NXES peak as labeled H', in which no corresponding UPS peak exists. The energy difference between the second NXES peak (H) and the peak H' is about 1.4 eV. Due to the presence of the chemical shift of the C sites in the molecule of about 1.3 eV (not shown), one may assign the peaks H and H' to the transitions from the HOMO to the ring and pyrrole C1s holes, respectively. However, this assignment cannot be applied to the N Kα NXES spectrum, which also shows the double peaks of H and H', since the chemical shift of the N sites in the molecule is only 0.2 eV (not shown).

As a possible origin of the peaks H and H' in the XES spectra, intermolecular interaction in the bulk phase may play a crucial role. For detailed discussion on relationship of the crystalline structure to the bulk electronic structure, the FY-XAS and XES experiments on amorphous films and single crystals of M-Pc molecules are now in progress.

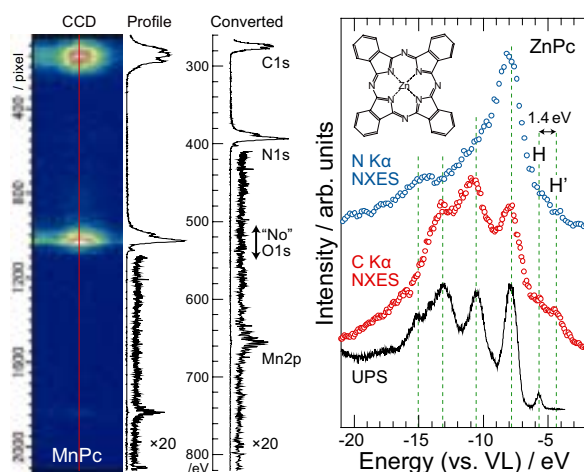


Fig. 1. (Left) The observed CCD image, its lineprofile, and a converted XES spectrum of the MnPc crystalline film. (Right) The C Kα and N Kα normal XES spectra of the 200-nm-thick ZnPc crystalline film, compared with a UPS spectrum of a 10-nm-thick ZnPc film.

[1] H.S. Kato *et al.*, UVSOR Act. Rep. **35** (2008) 114; a separate page in this volume.

[2] T. Hatsui *et al.*, AIP Conf. Proc. **705** (2004) 921; UVSOR Act. Rep. **34** (2007) 42.

## *In Situ* Magnetic Circular Dichroism Experiment on Ferromagnetic Semiconductor EuO Thin Films

H. Miyazaki<sup>1,2</sup>, T. Ito<sup>1,3</sup>, K. Terashima<sup>1</sup>, H. J. Im<sup>4</sup>, Y. Takagi<sup>3,5</sup>, T. Nakagawa<sup>3,5</sup>, Y. Yamamoto<sup>5</sup>, S. Kimura<sup>1,3</sup>, S. Yagi<sup>2</sup>, M. Kato<sup>2</sup>, K. Soda<sup>2</sup> and T. Yokoyama<sup>3,5</sup>

<sup>1</sup>*UVSOR Facility, Institute for Molecular Science, Okazaki 444-8585, Japan*

<sup>2</sup>*Graduate School of Engineering, Nagoya University, Nagoya 464-8603, Japan*

<sup>3</sup>*School of Physical Sciences, The Graduate University for Advanced Studies, Okazaki 444-8585, Japan*

<sup>4</sup>*Department of Advanced Physics, Hirosaki University, Hirosaki 036-8560, Japan*

<sup>5</sup>*Department of Molecular Structure, Institute for Molecular Science, Okazaki 444-8585, Japan*

Europium monoxide (EuO) is a ferromagnetic semiconductor with the Curie temperature ( $T_C$ ) at around 70 K [1, 2]. In the electron doping case by the Eu excess or substitute  $Gd^{3+}$  or  $La^{3+}$  from  $Eu^{2+}$  ion,  $T_C$  increases up to 150 K and the electrical resistivity drops twelve-order of magnitude below  $T_C$  originating in a metal-insulator transition (MIT) [2, 3]. To reveal the origin of these physical properties of EuO, it is important to clarify the relation of the electronic structure to the magnetic property. The soft X-ray Magnetic Circular Dichroism (XMCD) is powerful technique to determine the magnetic configuration of the electronic structure. Using this technique we observed the electronic structure of the Eu 4*f* states under the magnetic field.

Single-crystalline EuO thin films with a thickness of about 50 nm were fabricated by the molecular beam epitaxy (MBE) method. Epitaxial growth of the single-crystalline EuO thin films with the 1 x 1 EuO (100) patterns was confirmed with low energy electron diffraction (LEED) and reflection high energy electron diffraction (RHEED) methods. The  $T_C$  measured with a superconducting quantum interference device (SQUID) magnetometer was 71 K [4]. The *in situ* Eu  $M$ -edge X-ray adsorption spectra (XAS) and XMCD measurements were performed using a total electron yield mode at the bending magnet beamline 4B of UVSOR-II combined with the MBE system. The EuO thin films were prepared in the growth chamber and were transferred to the superconducting magnet chamber under the UHV condition.

Figure 1 shows the Eu  $M_{4,5}$  XAS of an EuO (100) thin film recorded at the temperature of 5 K and the magnetic field of  $\pm 1$  T. The magnetic field was applied perpendicular to the sample surface. Observed XAS spectra mainly have two structure at the photon energy 1130.6 and 1134.4 eV. Since the peaks from the  $Eu^{3+}$  3*d* states are not observed, the EuO does not contain impurities such as  $Eu_2O_3$ . The XMCD spectrum, which is obtained by the subtraction of the XAS spectrum of  $H = -1$  T from that of 1 T, is in good agreement with previously results and theoretical spectrum for a  $Eu^{2+}$  ion with  $L = 0$  and  $S = 7/2$  [6, 7].

To summarize, we succeeded to measure XMCD spectra of single-crystalline EuO thin films *in situ*. The method is good for the excluding the extrinsic effect such as oxidization, impurity and so on. The detailed analysis and the further study for EuO thin films are in progress.

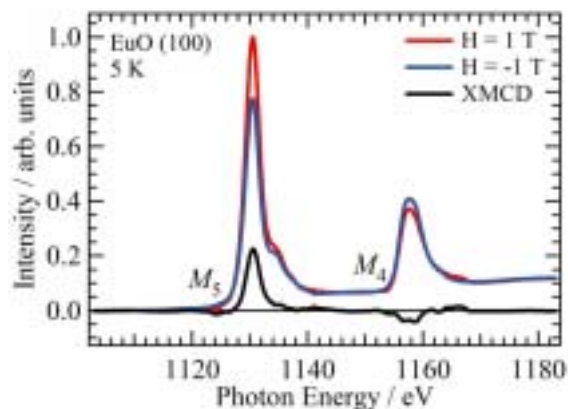


Fig. 1. Eu  $M_{4,5}$  XAS of EuO thin films recorded at 5 K with 1 (red line) and -1 T (blue line), respectively. The lowest curves (black line) shows the difference between both, which is called the XMCD spectrum.

[1] N. Tsuda *et al.*, *Electronic Conduction in Oxides* (Springers College) (1976).

[2] A. Mauger *et al.*, *J. Phys. (paris)* **39** (1978) 1125.

[3] Y. Shapira, S. Foner, and T. B. Reed, *Phys. Rev. B* **8** (1973) 2299. ; **8** (1973) 2316.

[4] H. Miyazaki *et al.*, *Jpn. J. Appl. Phys.* (2008) (in press).

[5] H. Lee *et al.*, *J. Appl. Phys.* **102** (2007) 053903.

[6] J. Holroyd *et al.*, *J. Appl. Phys.* **95** (2004) 6571.

[7] J. B. Goedkoop *et al.*, *Phys. Rev. B* **37** (1988) 2086.

## Ce 4d-4f Resonant Photoemission Studies in Ce Dilute Kondo System

H. J. Im<sup>1</sup>, M. Tsunekawa<sup>2,3,4</sup>, H. Miyazaki<sup>3,5</sup>, T. Ito<sup>3,6</sup>, S. Kimura<sup>3,6</sup>,  
K. E. Lee<sup>7</sup>, J. B. Hong<sup>7</sup> and Y. S. Kwon<sup>7</sup>

<sup>1</sup>Department of Advanced Physics, Hirosaki University, Hirosaki 036-8561, Japan

<sup>2</sup>Research Center for Materials Science, Nagoya University, Nagoya 464-8602, Japan

<sup>3</sup>UVSOR Facility, Institute for Molecular Science, Okazaki 444-8585, Japan

<sup>4</sup>Faculty of Education, Shiga University, Otsu 520-0862, Japan

<sup>5</sup>Graduate School of Engineering, Nagoya University, Nagoya 464-8603, Japan

<sup>6</sup>School of Physical Sciences, The Graduate University for Advanced Studies, Okazaki 444-8585, Japan

<sup>7</sup>Department of Physics, Sungkyunkwan University, Suwon 440-746, Korea

Localization of electrons in metals has been in the center of condensed matter physics. The intriguing phenomena take place, when the localized electrons hybridize with conduction electrons. For example, heavy fermion systems show a variety of the ground states from magnetic to non-magnetic states via the quantum critical point (QCP) as a function of the hybridization. In order to understand the localization in terms of electronic structure, we have performed resonant photoemission (RPES) studies of  $Ce_{1-x}Gd_xCoSi_3$ , where the ground state changes antiferromagnetism to non-magnetism via the QCP ( $x = 0.4$ ) [1]. In previous report, the large Kondo resonance (KR) peak near the Fermi-level ( $E_F$ ) is retained from  $x = 0$  to 0.6, indicating the continuous change of Ce 4f-character across the QCP unlike a local quantum critical scenario [2,3]. This gives rise to a long-standing fundamental question, i.e., how the KR peak behaviors in the different states (the periodic and impurity) of Ce 4f-electron and what the fate of the KR peak is in a dilute state.

In this report, Ce 4d-4f RPES measurements were carried out for the Ce-dilute system,  $Ce_{0.1}Gd_{0.9}CoSi_3$ , at BL5U. The used photon energies are 120 (on) and 113 eV (off). Total energy resolution is about 65 meV for the photon energies of 120 eV. Measurement temperature is 10 K. Sample surfaces were prepared by *in situ* fracturing under  $2 \times 10^{-8}$  Pa. Sample cleanliness is checked by the absence of oxidation peak around -6 and -10 eV.

Figure 1 shows the Ce 4d-4f on- and off-RPES spectra. The spectra are normalized to the intensity of Gd  $4f^6$  peak at  $\sim -8.4$  eV, whose cross-section should be almost the same in on- and off-photon energies. We observe the additional weight of the on-spectrum in valence band from -5 eV to  $E_F$  in comparison with the off-spectrum, indicating Ce 4f-state.

Figure 2 is the obtained Ce 4f-spectrum near  $E_F$  by subtraction of the off- from on-spectrum. The two peaks are clearly observed at about -0.2 eV and  $E_F$ , which are separated by spin-orbit interaction. The former is Ce  $4f_{7/2}^1$  final-state and latter Ce  $4f_{5/2}^1$  final-state (the tail of KR peak). Moreover, it is recognized that the intensity of KR peak is much

larger than that of Ce  $4f_{7/2}^1$  peak, indicating strong hybridization strength in Ce dilute Kondo system.

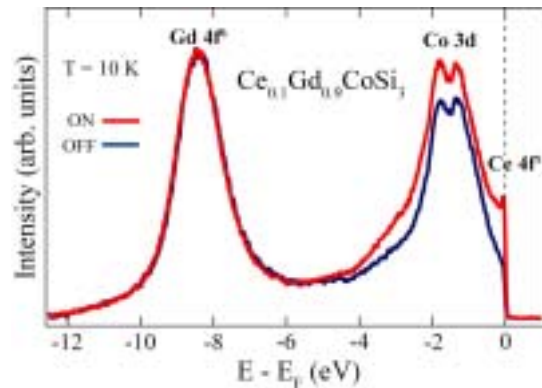


Fig. 1. Ce 4d-4f on- and off-RPES spectra of  $Ce_{0.1}Gd_{0.9}CoSi_3$ .

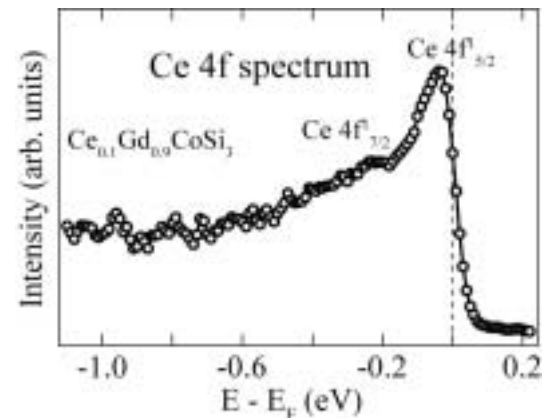


Fig. 2. Ce 4f spectrum of  $Ce_{0.1}Gd_{0.9}CoSi_3$ .

- [1] J. B. Hong *et al.*, Physica B **403** (2008) 911.
- [2] H. J. Im *et al.*, UVSOR Activity Report **35** (2008) 119.
- [3] H. J. Im *et al.*, Phys. Rev. B **72** (2005) 220405.

## Photoemission Study of CTAB-Passivated Au Nanorods

M. Imamura, A. Matsumoto, T. Kitagawa, S. Fujimasa and H. Yasuda

*Department of Mechanical Engineering, Kobe University, Kobe 657-8501, Japan*

Recently, chemically synthesized cetyltrimethyl ammonium bromide(CTAB)-passivated Au nanorods attract much attention due to their characteristic optical properties. CTAB-passivated Au nanorods are generally prepared with the seed-mediated growth method. The aspect ratio of Au nanorods is easily controlled by Ag ion concentration during the preparing process. However, the detailed structure of CTAB-passivated Au nanorod and the role of Ag in the growth process and are still unclear. In order to elucidate the structure of CTAB-passivated Au nanorod and the role of Ag ions, we have carried out the core-level photoemission study.

The CTAB-passivated Au nanorods are prepared by seed-mediated growth method developed by M. A. El-sayed *et al.*[1] We performed the X-ray and synchrotron-radiation photoemission measurements. The synchrotron photoemission study was carried out with the incident photon energy of 190 eV at BL-5U of UVSOR facility.

Figure 1 shows the Ag 3d core-level X-ray photoemission spectrum of CTAB-passivated Au nanorods with the aspect ratio of 4.1 supported on the HOPG substrate. The Ag 3d core-level photoemission spectrum measured from the bulk surface is also shown as a reference. The Ag 3d core-level X-ray photoemission spectrum of CTAB-passivated Au nanorods shifted to lower binding energy, and shows asymmetric spectral shape in the higher binding energy side compared with that of the bulk surface. In order to elucidate the chemical states of Au nanorods, we have carried out the line-shape analysis of the photoemission spectrum. The photoemission spectrum of Ag 3d in Au nanorods consists of two components. The higher binding energy component is considered to be the interface component that originates from the bonding between the Ag atoms and Br atoms, which indicates the passivation of Ag atoms by the CTAB molecule. The lower binding energy component in the photoemission spectrum of the Au nanorods shifted to lower binding energy side compared with the bulk component in the spectrum of bulk Ag, and is assigned as Au-Ag interface component. Thus, it is considered that Ag atoms are passivated by Br and bond to Au atoms of the nanorods.

Figure 2 shows the Au 4f photoemission spectrum of Au nanorods measured with synchrotron radiation light source. The results of the line shape analysis are also shown in the figure. As shown in Fig. 2, Au 4f photoemission spectrum of Au nanorods consist of one component, and no surface component appears. The disappearance of Au-Ag interface component in fig. 2 is consistent with the result of line-shape analysis of the Ag 3d spectrum. The charge transfer

between Au and Ag is considered to be very small, since the electron affinity of Au and that of Ag are quite similar. In addition, the volume fraction of Ag atoms are small compared with that of Au. Therefore Au-Ag interface component was not observed. From these results, it is concluded that Ag layer formed on the Au nanorod surface is monolayer, and the Ag layer is passivated by the CTAB molecules.

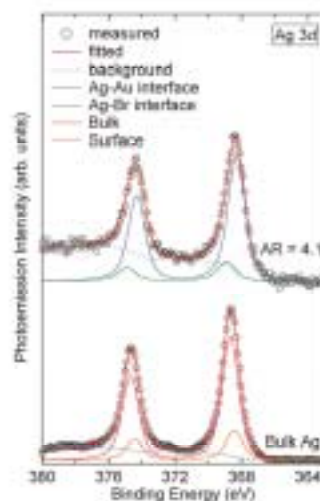


Fig. 1. Ag 3d core-level X-ray photoemission spectrum and the results of line shape analysis of CTAB-passivated Au nanorod with the aspect ratio of 4.1.

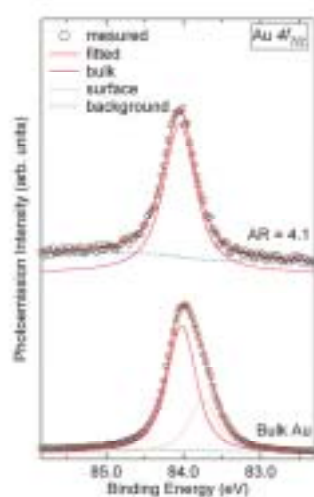


Fig. 2. Au 4f<sub>7/2</sub> core-level synchrotron photoemission spectrum and the results of line shape analysis of CTAB-passivated Au nanorod with the aspect ratio of 4.1.

[1] B. Nikoobakht and M.A. El-Sayed, *Chem. Mater.* **15** (2003) 1957.

## Ce 4d-4f Resonant Photoemission Study on Single-Crystalline Cerium

T. Ito<sup>1,2</sup>, H. Miyazaki<sup>1,3</sup>, S. Kimura<sup>1,2</sup> and K. Maesawa<sup>4</sup>

<sup>1</sup>UVSOR Facility, Institute for Molecular Science, Okazaki 444-8585, Japan

<sup>2</sup>School of Physical Sciences, the Graduate University for Advanced Studies (SOKENDAI), Okazaki 444-8585, Japan

<sup>3</sup>Graduate School of Engineering, Nagoya University, Nagoya 464-8603, Japan

<sup>4</sup>Department of Liberal Arts and Sciences, Toyama Prefectural University, Toyama 939-0398, Japan

Cerium is one of the most fascinating model systems to clarify the essential origin of strong electron correlations, causing the anomalous magnetic/electronic properties. This is because metallic cerium shows a unique first-order isostructural (fcc  $\rightarrow$  fcc) phase transition from the high-temperature  $\gamma$  phase to the low-temperature  $\alpha$  phase with a huge (15 %) volume reduction. According to the Kondo volume collapse theory based on the Anderson impurity model (AIM),  $\gamma$  -  $\alpha$  phase transition has been described by the change of the effective hybridization intensity of the conduction *spd* electrons with the *f* electron, from weak ( $\gamma$ ; localized) to strong ( $\alpha$ ; itinerant) one [1]. Photoemission spectroscopy has been used to directly estimate the applicability of AIM on various kinds of strongly correlated *f* electron systems by comparing the Kondo scaling parameter between the photoemission experiment and the AIM theory [2]. On the other hand, a recent angle-resolved photoemission (ARPES) result suggests that *f* states have band dispersions and cannot be treated as a local spin state based on AIM [3]. Thus the direct observation of the 4*f* band structure by using ARPES is indispensable to clarify the origin of  $\gamma$  -  $\alpha$  phase transition in cerium.

Figure 1 shows the change of valence band photoemission spectra of single-crystalline cerium as a function of Ar<sup>+</sup>-sputtering time. After 22 hours, extrinsic contamination peaks at 6.5 and 11 eV and CeO<sub>2</sub> features at 2 and 5 eV almost disappear, which can be attributed to successful cleaning of the sample surface. However, unexpected peak remained at 6eV. Though the origin of the peak is not clear at present, we think the peak is not come from CeO<sub>2</sub> but from chemically free oxygen contained in the single-crystalline cerium, since the peak intensity suddenly decreases at low temperature.

Figure 2 shows the temperature dependence of the on-resonant angle-integrated photoemission spectrum of the clean cerium above and below  $\gamma$  -  $\alpha$  phase transition temperature. According to AIM, the peaks at the Fermi level ( $E_F$ ) and 2.5 eV has been attributed to the spin-orbit splitted 4*f*<sup>1</sup> and the 4*f*<sup>0</sup> final states, respectively, originating from the strong *cf* hybridization [1]. We observed a sudden enhancement of 4*f*<sub>5/2</sub><sup>1</sup> peak below the transition

temperature, which is consistent with the previous study. To clarify the change of the electroic structure due to the  $\gamma$ - $\alpha$  transition, an ARPES measurement on the single-crystalline cerium will be performed in the near future.

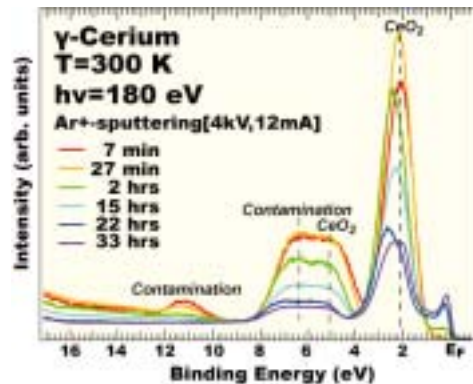


Fig. 1. Change of photoemission spectra due to the surface cleaning by the Ar<sup>+</sup>-sputtering measured at T=300 K using  $h\nu = 180$  eV photons.

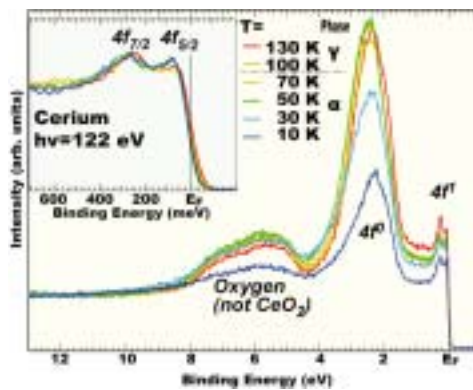


Fig. 2. Temperature-dependence of Ce 4*d*-4*f* on-resonance spectra ( $h\nu=120$  eV). (Inset) the enlargement near  $E_F$ . The intensities are normalized at 4*f*<sub>7/2</sub><sup>1</sup>.

[1] J. W. Allen *et al.*, Adv. Phys. **35** (1986) 275.

[2] D. Malterre, M. Gioni and Y. Baer, Adv. Phys. **45** (1996) 299.

[3] H. J. Im *et al.*, Phys. Rev. Lett. **100** (2008) 176402.

## Electronic Structure of $\text{Ba}_3\text{Co}_2\text{O}_6(\text{CO}_3)_{0.7}$

M. Kikuchi<sup>1</sup>, S. Ogawa<sup>1</sup>, H. Miyazaki<sup>2</sup>, M. Inukai<sup>2</sup>, K. Iwasaki<sup>2</sup>, T. Matsui<sup>2,3</sup>, M. Kato<sup>2</sup>,  
S. Yagi<sup>2</sup> and K. Soda<sup>2</sup>

<sup>1</sup>*School of Engineering, Nagoya University, Nagoya 464-8603, Japan*

<sup>2</sup>*Graduate School of Engineering, Nagoya University, Nagoya 464-8603, Japan*

<sup>3</sup>*EcoTopia Science Institute, Nagoya University, Nagoya 464-8603, Japan*

Cobalt oxides such as  $\text{Na}_x\text{CoO}_2$  have received much attention because of their fascinating transport and magnetic properties. Recently it has been found that a barium cobalt oxycarbonate  $\text{Ba}_3\text{Co}_2\text{O}_6(\text{CO}_3)_{0.7}$  shows metallic behavior of its electric conductivity above 300 K and fairly large power factor of 0.9  $\text{mWm}^{-1}\text{K}^{-2}$  at 300 K with positive thermoelectric power of about 120  $\mu\text{VK}^{-1}$  [1].  $\text{Ba}_3\text{Co}_2\text{O}_6(\text{CO}_3)_{0.7}$  has pseudo-one dimensional structure with Co-O chains consisting of face-sharing  $\text{CoO}_6$  octahedra along the  $c$  axis. In the present study, we have investigated its electronic structure by photoelectron spectroscopy, in order to understand the physical properties.

Single crystalline specimens of  $\text{Ba}_3\text{Co}_2\text{O}_6(\text{CO}_3)_{0.7}$  in size of 5 x 0.5 x 0.5  $\text{mm}^3$  was prepared by a flux method [1], and their clean surfaces for photoelectron measurement was obtained by *in situ* cleaving the specimens in perpendicular to the  $c$  axis.

Valence band photoelectron spectra recorded at 20 K are summarized in Fig. 1. Excitation photon energy  $h\nu$  is indicated in the right side of each spectrum, and each spectrum is normalized with the integrated intensity. We recognize features A to H in the spectra; we ascribe the features A to C to the hybridized bands of the Co 3d and O 2p states, comparing with reported spectra of  $\text{Na}_x\text{CoO}_2$  [2], which is composed of triangular planes of edge-sharing  $\text{CoO}_6$  octahedra. The resonance behavior at the Co 3p threshold around  $h\nu = 60 \sim 70$  eV indicates the relatively large characters of Co 3d states to the features A and B and of the O 2p state to the feature C. The bands D, F, G and H are assigned to the  $\text{CO}_3$ -derived states, Ba 5p spin-orbit doublets and O 2s state, respectively. We ascribe the feature E to the surface components.

Figure 2 shows detailed spectrum near the Fermi level  $E_F$  measured at 20 K and  $h\nu = 40$  eV in comparison with a reference Au spectrum. The spectrum of  $\text{Ba}_3\text{Co}_2\text{O}_6(\text{CO}_3)_{0.7}$  reveals large reduction in intensity towards  $E_F$  but clear finite intensity at  $E_F$ . This may suggest the electron doping into the low-spin bands of  $\text{Co}^{4+}(t_{2g} 3d^5)$ , which in turn might lead to the positive thermoelectric power of 81 or 141  $\mu\text{VK}^{-1}$  at high temperatures for the  $\text{Co}^{4+}$  concentration  $x$  of 0.7 [3], consistent with the observed value.

A 1/8-power-law dependence on the binding energy, which may be expected in one-dimensional fermion system [4], is also shown in Fig. 2 after the convolution with a Gaussian function presenting an experimental energy resolution of 34 meV. It seems to

explain the spectral feature near  $E_F$  fairly well. For definite conclusion, further study is intended with an improved energy resolution and statistics.

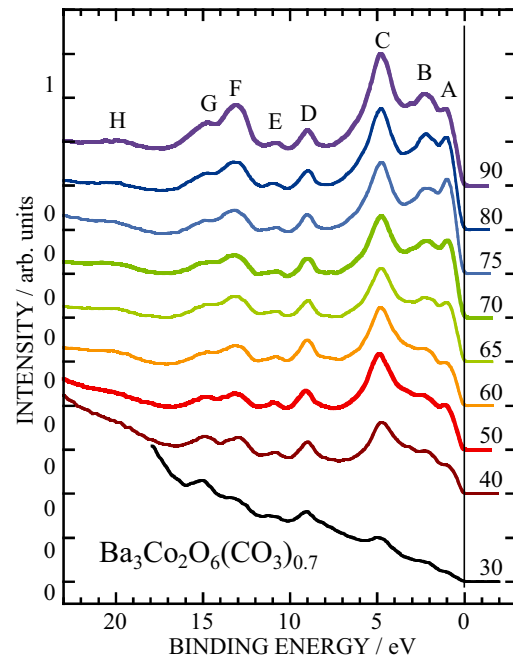


Fig. 1. Valence-band spectra of  $\text{Ba}_3\text{Co}_2\text{O}_6(\text{CO}_3)_{0.7}$ .

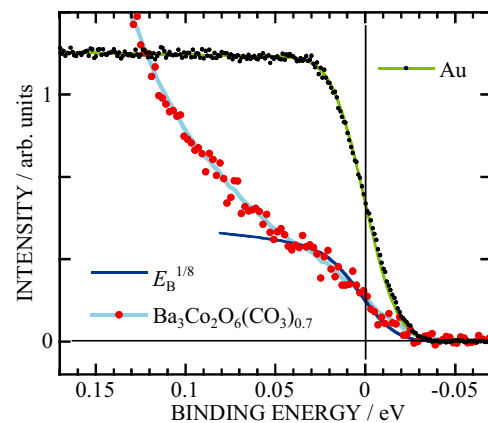


Fig. 2. Detailed spectra near the Fermi level.

[1] T. Yamamoto *et al.*, Proc. Int. Symp. on EcoTopia Science 2007, p.145.

[2] M. Z. Hasan *et al.*, Phys. Rev. Lett. **92** (2004) 246402.

[3] W. Koshibae *et al.*, Phys. Rev. B **62** (2000) 6869.

[4] J. Voit, Pep. Prog. Phys. **57** (1994) 977.

## Temperature Dependent Angle-Resolved Photoemission Spectra of La-Doped EuO

H. Miyazaki<sup>1,2</sup>, T. Ito<sup>1,3</sup>, K. Terashima<sup>1</sup>, H. J. Im<sup>4</sup>, S. Yagi<sup>2</sup>, M. Kato<sup>2</sup>, K. Soda<sup>2</sup>  
and S. Kimura<sup>1,3</sup>

<sup>1</sup>UVSOR Facility, Institute for Molecular Science, Okazaki 444-8585, Japan

<sup>2</sup>Graduate School of Engineering, Nagoya University, Nagoya 464-8603, Japan

<sup>3</sup>School of Physical Sciences, The Graduate University for Advanced Studies, Okazaki 444-8585, Japan

<sup>4</sup>Department of Advanced Physics, Hirosaki University, Hirosaki 036-8560, Japan

Pristine europium monoxide (EuO) is a ferromagnetic semiconductor with the Curie temperature ( $T_C$ ) at around 70 K [1, 2]. In the electron doping case by the Eu excess or substitute  $Gd^{3+}$  or  $La^{3+}$  from  $Eu^{2+}$  ion,  $T_C$  increases up to 150 K and the electrical resistivity drops twelve-order of magnitude below  $T_C$  originating in a metal-insulator transition (MIT) [2, 3]. Recently, we reported that the origin of the magnetic properties of EuO is caused by the hybridizations of the Eu  $4f$ –O  $2p$  and Eu  $4f$ – $5d$  [4, 5]. To reveal the origin of increase of  $T_C$  due to the electron doping, it is important to clarify the electronic structure. Three dimensional angle-resolved photoemission spectroscopy (3D-ARPES) using a synchrotron radiation is the most powerful technique to directly determine the electronic band structure. Using this technique we observed the change of the electronic structure across  $T_C$ .

Single-crystalline La-doped EuO thin films with a thickness of about 50 nm were fabricated by a molecular beam epitaxy (MBE) method. Epitaxial growth of the single-crystalline La-doped EuO thin films with the  $1 \times 1$  EuO (100) patterns was confirmed by a low energy electron diffraction (LEED) method.  $T_C$  measured with a superconducting quantum interference device (SQUID) magnetometer was around 200 K. The 3D-ARPES measurements were performed at the beam line 5U of UVSOR-II combined with the MBE system. The total energy and momentum resolutions for the ARPES measurement were set 123 meV and  $0.020 \text{ \AA}^{-1}$  at the  $\Gamma$  point and 45 meV and  $0.014 \text{ \AA}^{-1}$  at the X point, respectively.

Figures 1 (a) and (b) show the 3D-ARPES results for La-doped EuO near the  $\Gamma$  and X points, respectively. The local minimums on the second-derivative energy distribution curves (EDCs) indicate the peaks and shoulders of the EDCs. EDCs at binding energies ( $E_B$ ) of 0.5 – 3.5 eV and of 4.0 – 6.5 eV are attributed to the Eu  $4f$  and O  $2p$  states, respectively. In comparison with the temperature-dependent 3D-ARPES spectra of pristine EuO [6], the temperature dependence is similar, but the photoemission intensity near the Fermi energy ( $E_F$ ,  $E_B = 0$  eV) at the X point appears indicating the metallic electronic structure. Since there is no intensity at  $E_F$  at the  $\Gamma$  point, the conduction band has the momentum dependence. According to the

electronic resistivity data of an electron-doped EuO [2, 3], metallic electronic structure is expected to appear only below  $T_C$ . Though the origin of the observed conduction band is not clear yet, therefore, the doped electrons may appear in the ARPES spectrum and play an important role for the increasing of  $T_C$ . The detailed analysis and the further study for electron-doped EuO thin films are in progress.

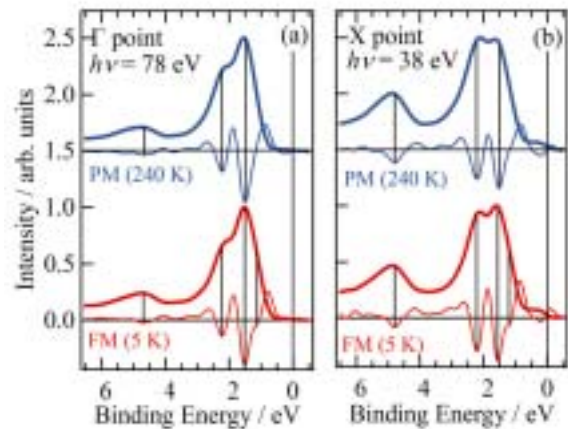


Fig. 1. Temperature dependence of the energy distribution curves (EDCs, thick line) and their second-derivative EDCs (thin line) of a La-doped EuO (100) thin film at the  $\Gamma$  (a) and X (b) points.

- [1] N. Tsuda *et al.*, Electronic Conduction in Oxides (Springers College) (1976).
- [2] A. Mauger *et al.*, J. Phys. (paris) **39** (1978) 1125.
- [3] Y. Shapira, S. Foner, and T. B. Reed, Phys. Rev. B **8** (1973) 2299.; **8** (1973) 2316.
- [4] H. Miyazaki *et al.*, Physica B **403** (2008) 917.
- [5] H. Miyazaki *et al.*, Jpn. J. Appl. Phys. (2009) (in press).
- [6] H. Miyazaki *et al.*, submitted.

## Dilute Multi Ferroic Semiconductor GaCrN

S. Emura<sup>1</sup>, K. Tokuda<sup>1</sup>, H. Tambo<sup>1</sup>, F. Suzuki<sup>2</sup> and K. Fukui<sup>2</sup>

<sup>1</sup>*ISIR, Osaka University, Mihoga-oka 8-1, Ibaraki, Osaka 567-0047, Japan*

<sup>2</sup>*Faculty of Engineering, University of Fukui, Bunkyo 3-9-1, Fukui 910-8507, Japan*

Multi-ferroic materials, which simultaneously show ferro-magnetism, ferro-electricity, and ferro-elasticity or two of those, and exist the coupling among them, attract much attention because of the physical interest in the coupling mechanism and for the potentiality of the various applications. We may be opening the door of new materials in the multi-ferroic research field, that is, dilute multi-ferroic semiconductors (DMS). Here, we will describe on DMS, GaCrN (GaN:Cr), where the Cr ion is a dilute dopant up to ~1.5%. In higher concentration, multi-ferroic phenomena are quenched (concentration quenching). This dilute alloy GaCrN is well known as a dilute magnetic semiconductor. The specimen studied here is a single crystal in the thin layer form on an Al<sub>2</sub>O<sub>3</sub> substrate.

Analysis of XAFS spectra around Cr K-edge leads to the discovery the spontaneous elastic deformation (quasi Jahn – Teller effect) involving the local electric polarization. The polarization dependence of the absorption spectra in VUV energy region gives the evidence of the ordering of the elastic deformation and consequently of the electric polarization.

Figure 1 presents the radial distribution functions (RDFs) from the Cr ion site. We can see a doublet peak at around 1.3 ~ 1.7Å corresponding to Cr – N bonds and a single peak at 2.9Å corresponding to Cr – Ga bond. This finding means that there exist two different lengths for the first nearest neighbor (Cr – N), and one distance for the second nearest neighbor (Cr – Ga), resulting in the simply parallel shift of the four nitrogen ions as shown in Fig. 2. This deformation is originated in quasi Jahn – Teller effect. Involving the deformation, it is apparent from the figure that the local spontaneous electric polarization is induced around the doped Cr ion. Here, it should be noticed that there are four nearly equivalent legs because the original site symmetry is nearly T<sub>d</sub>, and we cannot distinguish these four legs from the XAFS analysis, which merely gives the one-dimensional structural information. The parallel shifts may randomly be distributed in the matrix or ordered along some direction of the matrix. The answer will come from the polarization effect of the absorption spectra. Figure 3 shows the incident angle dependence of the absorption spectra in VUV region observed at BL5B at UVSOR. At zero angles, the electric field of incident photon is vertical to the crystal c-axis of GaCrN. The absorption band around 28 nm (44.3 eV), which is tentatively assigned to the transition from 3p of the Cr atom to the s-like conduction band of matrix because of the wide halfwidth, strongly depends on the direction of the

electric polarization of the incident photon. In the parallel electric field to the c-axis, the band vanishes, indicating anisotropy along the c-axis. This is clear evidence of the ordering of the deformation and consequent electric polarization.

The GaCrN alloy is one of the dilute magnetic semiconductors. From our observation, it is found that it behave as a ferro-electric and elastic material [1]. The coupling among those leads to substances of a new category in multi-ferroic research field.

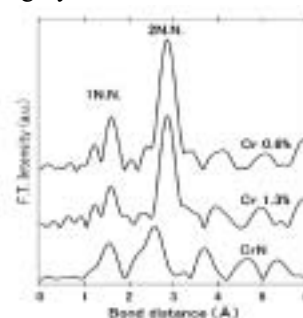


Fig. 1. RDFs from Cr ion site.

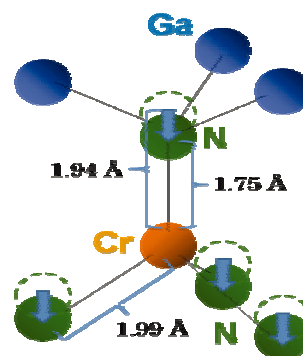


Fig. 2. Schematic drawing of relative positions.

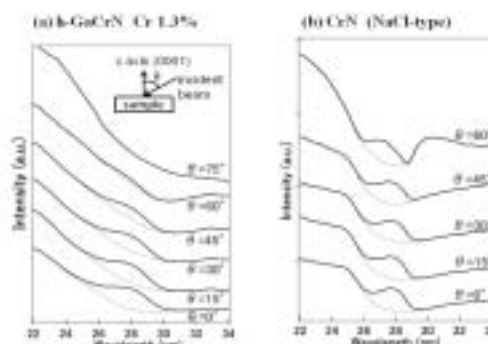


Fig. 3. Angular dependence of the absorption.

[1] submitted to Phys. Rev. Lett.

## Terahertz Spectroscopy of Bromides-Doped Silver Phosphate Superionic Conducting Glasses

T. Awano

*Department of Electronic Engineering, Tohoku Gakuin University, Tagajo 985-8537, Japan*

The enhancement of ionic conductivity by metal iodide doping into silver phosphate glass has been reported with  $\text{BiI}_3$ ,  $\text{CdI}_2$  and other metal iodides [1]. The increase of ionic conductivity is proportional to dopant concentration and valence number of the metal ion. Meanwhile, silver bromide-doped silver phosphate glass has less ionic conductivity than the iodide-doped one [2]. These facts suggest the following mechanism of the enhancement of ionic conductivity; the doped metal ion substitutes silver ions which was connected with non-bonding oxygen according to their valence and the released silver ions contribute to ionic conduction. The halogen ions expand conduction channel for the silver ion between glass network chains of  $\text{PO}_4$  tetrahedra. This expansion is small in the case of bromide-doping therefore the conduction channel is narrow than in the case of iodide-doping. This abstract reports results of far-infrared spectra of metal bromides doped silver phosphate glasses to confirm the above mentioned model.

Figure 1 shows absorption spectra of  $(\text{AgBr})_x(\text{AgPO}_3)_{1-x}$  glass obtained from reflectivity spectra. Intensity of the band around  $120 \text{ cm}^{-1}$  increases as the bromine content increases. Peak position shifts slightly from  $113 \text{ cm}^{-1}$  ( $x=0.4$ ) to  $120 \text{ cm}^{-1}$  ( $x=0.1$ ).

Figure 2 shows absorption spectra of  $(\text{BiBr}_3)_{0.05}(\text{AgPO}_3)_{0.95}$  glass obtained from reflectivity spectra. Fig. 3 shows absorption spectra of  $(\text{CdBr}_2)_{0.1}(\text{AgPO}_3)_{0.95}$  glass. Intensity of the band around  $120 \text{ cm}^{-1}$  is almost the same as that of  $(\text{AgBr})_{0.4}(\text{AgPO}_3)_{0.6}$  glass in Fig. 1. Peak positions in Figs. 2 and 3 are around  $130 \text{ cm}^{-1}$  and different from that of  $(\text{AgBr})_{0.4}(\text{AgPO}_3)_{0.6}$  glass.

In the above mentioned model of structural change of the glass, the number of the released silver ions is proportional to the dopant concentration and also the valence number of the doped metal ion. Therefore intensities of newly induced absorption band by Ag-Br is expected to be proportional to the product of the dopant concentration and the valence number. On the other hand, intensities of newly induced absorption band by Cd- or Bi-O is expected to be proportional only to the dopant concentration. The intensity of Ag-O vibration should also decrease with the product of the dopant concentration and the valence number. The far-infrared spectral change seems to coincide with such mechanism of the structural change of the glass.

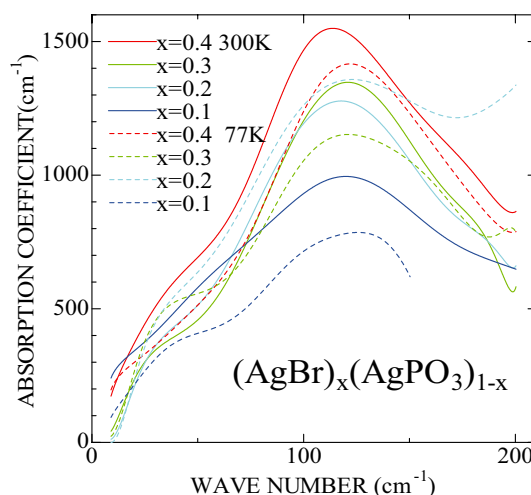


Fig. 1. Absorption spectra of  $\text{AgBr-AgPO}_3$  glasses obtained from reflectivity.

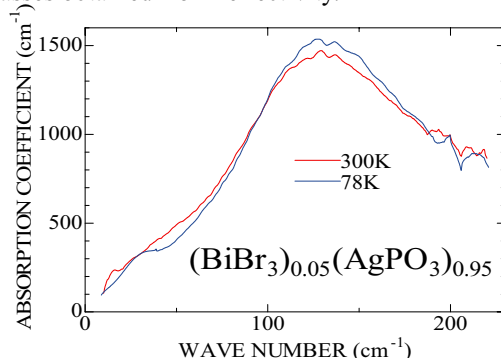


Fig. 2. Absorption spectra of  $\text{BiBr}_3\text{-AgPO}_3$  glass obtained from reflectivity.

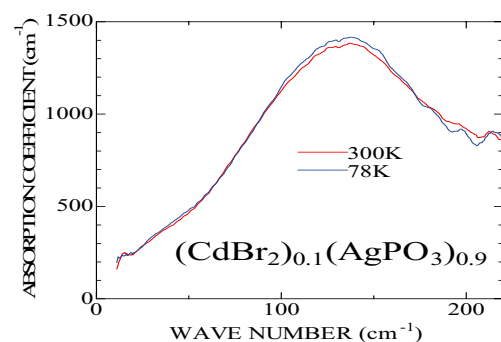


Fig. 3. Absorption spectra of  $\text{CdBr}_2\text{-AgPO}_3$  glass obtained from reflectivity.

- [1] H. Takahashi, H. Nakanii and T. Sakuma, *Solid State Ionics* **176** (2005) 1067.  
 [2] M. Hanaya, T. Okubayashi, T. Sakurai and M. Oguni, *Thermochimica Acta* **266** (1995) 79.

# Pressure-Dependent Far-Infrared Reflectivity Spectra of CeIn<sub>3</sub> at 9K

T. Iizuka<sup>1</sup>, T. Mizuno<sup>1</sup>, K. E. Lee<sup>2</sup>, H. J. Im<sup>3</sup>, T. Ito<sup>4,1</sup>, Y. S. Kwon<sup>2</sup> and S. Kimura<sup>4,1</sup>

<sup>1</sup>*School of Physical Sciences, The Graduate University for Advanced Studies (SOKENDAI), Okazaki 444-8585, Japan*

<sup>2</sup>*Department of Physics, Sungkyunkwan University, Suwon 440-746, Korea*

<sup>3</sup>*Department of Advanced Physics, Hirosaki 036-8561, Japan*

<sup>4</sup>*UVSOR Facility, Institute for Molecular Science, Okazaki 444-8585, Japan*

## Introduction

In recent years, some compounds called "heavy fermion"(HF) attract attention because of their various physical properties, which originate from the hybridization between itinerant conduction electrons and local 4*f* electrons. One of the characteristic physical properties is unconventional superconductivity due to HF, which appears near a quantum critical point (QCP) located in between the local and itinerant characters of 4*f* electrons.

CeIn<sub>3</sub> has an AuCu<sub>3</sub>-type simple cubic crystal structure with the ground state located in the local regime ( $T_N = 10$  K). With applying pressure, due to the increasing of the hybridization intensity between the conduction and 4*f* electrons, the ground state can be changed from antiferro magnetic (AFM) to nonmagnetic HF state via QCP. So CeIn<sub>3</sub> is one of suitable samples to study the hybridization dependence of electron structure near QCP. From the result of a de Haas-van Alphen (dHvA) effect measurement of CeIn<sub>3</sub> at 82 mK [1], the effective mass is enhanced at around the AFM ordering pressure of  $P_C = 2.6$  GPa. On the other hand, another typical material located near QCP, YbRh<sub>2</sub>Si<sub>2</sub>, has another boundary ( $T^*$ ) at which the carrier density probed by the Hall coefficient measurement drastically changes [2]. To reveal the relation of the mass enhancement of CeIn<sub>3</sub> to the enhancement of the carrier density of YbRh<sub>2</sub>Si<sub>2</sub> at  $T^*$ , the pressure-dependent reflectivity spectrum in the terahertz (THz) region below  $T_N = 10$  K were measured.

## Experimental

Single phase CeIn<sub>3</sub> samples were synthesized by an arc melting method under argon atmosphere, and then annealed at 600 °C for three weeks inside an evacuated quartz tube. The THz reflection spectroscopy under pressure was performed at the THz micro-spectroscopy end station of UVSOR-II BL6B. A diamond anvil cell was employed to produce high pressure. KBr and Au film were used for media and for a background spectrum, respectively.

## Results and Discussion

We obtained pressure-dependent reflectivity spectra [ $R(\omega, P)$ ] of CeIn<sub>3</sub> at 9.5 K in the pressure region from 0.6 to 3.3 GPa as shown in Fig. 1. All spectra were divided by that at 2.0 GPa to highlight the pressure dependence. With increasing pressure,

$R(\omega, P)$  of CeIn<sub>3</sub> mainly changes below 300 cm<sup>-1</sup> region. To derive the pressure dependence of the spectra, the spectrum is divided into three parts, and the integrated intensities of each area are plotted as a function of pressure in Fig. 2. The area at around 150 cm<sup>-1</sup> has a bottom at around 2.5 GPa and recovers above the pressure, in spite that the other lines monotonically increase with increasing pressure. The pressure of 2.5 GPa is close to the QCP of CeIn<sub>3</sub>. The spectral change suggests that the Drude weight of heavy quasiparticles enhance below 150 cm<sup>-1</sup> near the QCP and become smaller in the HF region. This result is consistent with the mass enhancement of CeIn<sub>3</sub> at QCP and the increasing of the carrier density at  $T^*$  in YbRh<sub>2</sub>Si<sub>2</sub>, i.e., a large Fermi surface due to the heavy quasiparticles appears at  $P_C$ . One possibility of the origin is the valence transition from Ce<sup>3+</sup> to Ce<sup>4+</sup> at  $P_C$ .

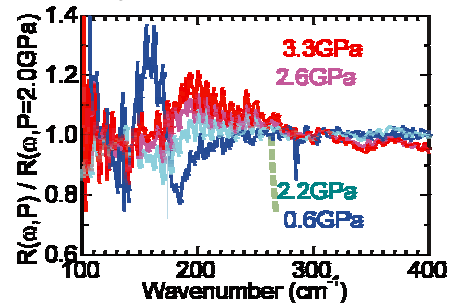


Fig. 1. Pressure-dependent reflectivity spectra  $R(\omega, P)$  divided by  $R(\omega, P = 2.0$  GPa) at 9.5K.

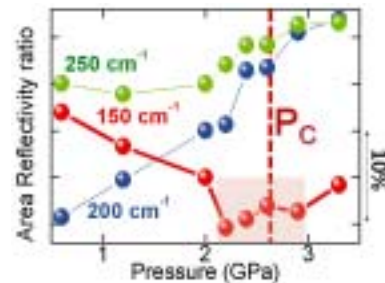


Fig. 2. The pressure dependence of the areas classified in Fig.1. Successive curves are offset by 5 % for clarity.  $P_C$  is the pressure of the QCP.

[1] R. Settai *et al.*, J. Phys. Soc. Jpn. **74** (2005) 3016.

[2] S. Paschen *et al.*, Nature **432** (2004) 881.

## Phonon-Polariton of GaN Observed by Far-Infrared Synchrotron Radiation

T. Inushima<sup>1</sup>, Y. Ota<sup>1</sup>, T. Yanagawa<sup>2</sup> and K. Fukui<sup>2</sup>

<sup>1</sup>*Department of Electronics, Tokai University, Hiratsuka, 259-1292, Japan*

<sup>2</sup>*Department of Electronics and Electrical Engineering, University of Fukui, Fukui 910-8507, Japan*

Temperature dependence of the reflectivity of GaN with a film thickness from 1 to 4  $\mu\text{m}$  is investigated from 50 to 750  $\text{cm}^{-1}$  by means of infrared synchrotron radiation. The phonon-polariton of GaN is observed in the energy range below  $E_1(\text{TO})$  phonon. From the temperature dependence of the damping factor of the phonon, it is found that the  $E_1(\text{TO})$  phonon decays primarily into phonons with a renormalized frequency of 226  $\text{cm}^{-1}$ . Compared with the damping factor of superconducting InN, GaN grown on sapphire has more defects in the film.

All of the GaN films investigated have a hexagonal structure and their c-axes are perpendicular to the sapphire (0001) planes. Therefore, one  $E_1$  optical phonon is observed in this configuration. Figure 1 shows the reflectivity spectrum of GaN with a thickness of 4  $\mu\text{m}$ . A clear Reststrahlen band is seen above 560  $\text{cm}^{-1}$ , which is due to the  $E_1$  optical phonon. The spectrum is analyzed using the following dielectric function,

$$\varepsilon(\omega) = \varepsilon_\infty - \frac{(\varepsilon_0 - \varepsilon_\infty)\omega_{\text{TO}}^2}{\omega^2 - \omega_{\text{TO}}^2 + i\omega\Gamma}. \quad (1)$$

Using Eq. (1), the reflectivity spectrum is well reproduced and obtained fitting parameters are given in the figure.

The phonon-polariton is observed below the  $E_1(\text{TO})$  phonon in Fig. 1, from which the damping factor  $\Gamma$  is obtained as a function of temperature shown in Fig. 2. The  $\Gamma$  of InN is also plotted for comparison. The  $\Gamma$  is the energy dissipation factor of the  $E_1(\text{TO})$  oscillation and  $1/\Gamma$  is regarded as the phonon lifetime. The lifetime was explained by Klemens in terms of a three-phonon process[1]. The three-phonon process is a decay process of the zone-center TO or LO phonon into two LA or TA phonons of equal frequencies and opposite wave vectors. In this consideration the temperature dependence of the  $\Gamma$  is expressed by the following equation;

$$\Gamma = \Gamma_0 + \Gamma_1 \coth\left(\frac{\hbar\omega_0}{2kT}\right). \quad (2)$$

As is shown in Fig. 2,  $\Gamma(T)$  is reproduced by  $\omega_0=226$   $\text{cm}^{-1}$  and 0.2 and 0.5 meV for  $\Gamma_0$  and  $\Gamma_1$ , respectively. This indicates that the  $E_1(\text{TO})$  phonon decays into two TA phonons with  $\omega_0=226$   $\text{cm}^{-1}$ . As the value of  $\Gamma_0$  is a measure of the defects in GaN, the measurement of the phonon-polariton is a tool for

examining the crystal quality dynamically.

The ratio of  $\Gamma/\omega_{\text{TO}}$  is the energy dissipation rate for the  $E_1$  vibration and is  $1.0 \times 10^{-2}$  for GaN and  $3.3 \times 10^{-3}$  for InN. When we regard this as an unharmonic factor of the crystal, GaN grown on sapphire has much dislocation than InN.

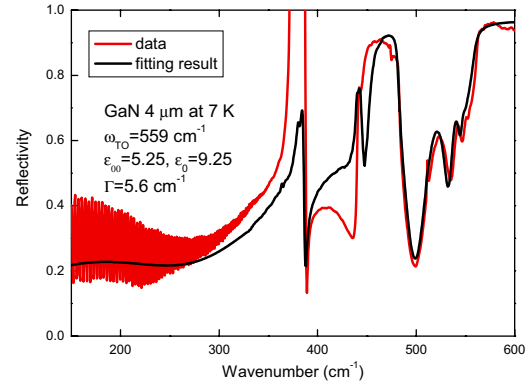


Fig. 1. Reflection spectrum of GaN at 7 K. The fitted line (black line) is drawn using Eq. (1). The fitting parameters are;  $\omega_{\text{TO}}=559$   $\text{cm}^{-1}$ ,  $\varepsilon_\infty=5.25$ ,  $\Gamma=0.0007$  eV,  $d=3.9$   $\mu\text{m}$ .

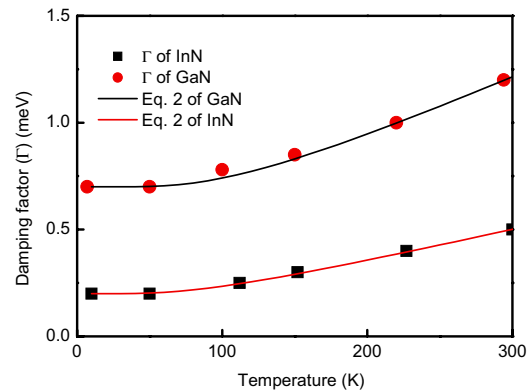


Fig. 2. Temperature dependence of the damping factors ( $\Gamma$ ) of GaN and those of InN. The fitting is done using Eq. (2). For GaN,  $\Gamma_0$  and  $\Gamma_1$  are 0.2 and 0.5 meV, respectively and  $\omega_0=226$   $\text{cm}^{-1}$  is obtained. As for InN,  $\Gamma_0$  and  $\Gamma_1$  are 0 and 0.2 meV, respectively, and  $\omega_0=177$   $\text{cm}^{-1}$  is obtained.

[1] P. G. Klemens, Phys. Rev. **148** (1966) 845.

## Origin of Middle-Infrared Peaks in CePd<sub>3</sub>

S. Kimura<sup>1,2</sup>, T. Iizuka<sup>2</sup> and Y. S. Kwon<sup>3</sup>

<sup>1</sup>*UVSOR Facility, Institute for Molecular Science, Okazaki 444-8585, Japan*

<sup>2</sup>*School of Physical Sciences, The Graduate University for Advanced Studies (SOKENDAI), Okazaki 444-8585, Japan*

<sup>3</sup>*Department of Physics, Sungkyunkwan University, Suwon 440-746, Korea*

Heavy fermion as well as mixed-valence materials, such as cerium (Ce), ytterbium (Yb), and uranium compounds, commonly have a characteristic peak structure (namely, the mid-IR peak) in the middle-infrared (mid-IR) region below 1 eV in their optical conductivity [ $\sigma(\omega)$ ] spectra [1]. The origin of the mid-IR peak has remained a long debated issue so far. To investigate the origin of the mid-IR peaks of Ce compounds, we calculate the  $\sigma(\omega)$  spectrum of CePd<sub>3</sub>, which is a typical heavy fermion material, from the first principle band calculation with the spin-orbit interaction (SOI).

Band structure calculation was performed by the full potential linearized augmented plane wave plus local orbital (LAPW+lo) method including SOI implemented in the WIEN2K code [2]. CePd<sub>3</sub> forms a Cu<sub>3</sub>Au-type cubic crystal structure (*Pm3m*, No. 221) with lattice constants of 4.1280 Å [3]. The band structure and  $\sigma(\omega)$  spectrum of LaPd<sub>3</sub> (lattice constant = 4.235 Å [4]) were also calculated for reference.

The calculated  $\sigma(\omega)$  spectra with and without SOI are plotted in Fig. 1. The experimental  $\sigma(\omega)$  spectrum of CePd<sub>3</sub> at T = 8 K [5] is also plotted in the figure. The experimental spectrum has three large peaks at 0.25, 0.55, and 0.78 eV, and one small peak at 0.04 eV. The calculated  $\sigma(\omega)$  spectrum with SOI also has three peaks at 0.3, 0.56, and 0.75 eV and one shoulder at 0.1 eV, despite the very low  $\sigma(\omega)$  intensity of LaPd<sub>3</sub>. This structure can be assigned to the experimental structure as follows: The peaks mainly appear in the  $\Gamma$ -X-R-M plane in the first Brillouin zone and the initial state of all peaks is commonly the highly dispersive conduction band [6]. The peaks at 0.3 and 0.78 eV in the calculated spectrum originate from the optical transitions to the Ce 4f<sub>7/2</sub> state near the  $\Gamma$ -point and near the bottom of the  $\Lambda$ -axis, respectively. The small peak at 0.55 eV originates from the transition near the  $\Delta$ - and S-axes. The shoulder structure at 0.1 eV in the calculation originates from the transition from the occupied flat band to the unoccupied Ce 4f<sub>5/2</sub> state near the  $\Gamma$ -point. Therefore, all of the mid-IR peaks of CePd<sub>3</sub> can be explained by the band structure calculation with SOI.

In the calculated spectrum without SOI, one large peak at 0.7 eV appears, as shown in Fig. 1. The spectrum cannot reproduce the experimental triple-peak structure. The SOI of the Ce 4f state

therefore plays an important role in the mid-IR triple-peak structure of CePd<sub>3</sub>; i.e., the mid-IR peaks originate from the band structure including the SOI of the Ce 4f state [7].

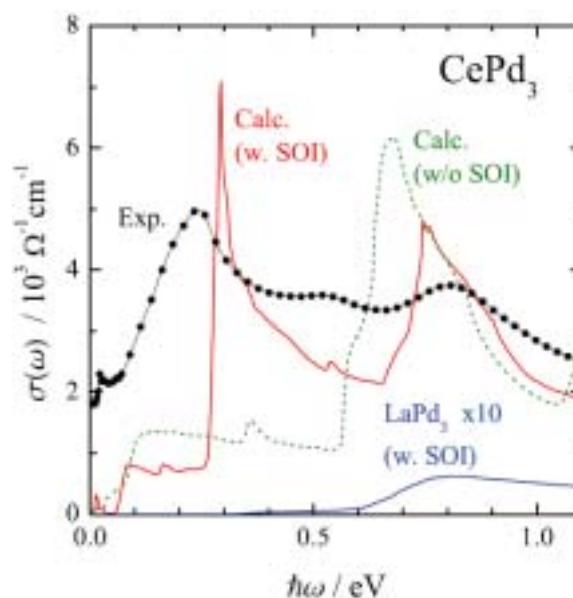


Fig. 1. Experimental and calculated optical conductivity [ $\sigma(\omega)$ ] spectra of CePd<sub>3</sub>. The calculated  $\sigma(\omega)$  spectrum of LaPd<sub>3</sub> is also plotted for reference. Two different calculations with and without SOI were performed. The experimental spectrum, which was obtained at T = 8 K, is derived from that reported elsewhere [5].

- [1] L. Degiorgi, *Rev. Mod. Phys.* **71** (1999) 687.
- [2] P. Blaha, K. Schwarz, P. Sorantin and S. B. Trickey, *Comput. Phys. Commun.* **59** (1990) 399.
- [3] K. H. J. Buschow, *Rep. Prog. Phys.* **42** (1979) 1373.
- [4] C. Koenig and M. A. Khan, *Phys. Rev. B* **38** (1988) 5887.
- [5] S. Kimura, H. Iwata, K. Kanai, S. Shin, G. Schmerber, J. P. Kappler and J. C. Parlebas, *Acta Phys. Pol. B* **34** (2003) 975.
- [6] A. Hasegawa and A. Yanase, *J. Phys. Soc. Jpn.* **56** (1987) 3990.
- [7] S. Kimura, T. Iizuka and Y. S. Kwon, *J. Phys. Soc. Jpn.* **78** (2009) 013710.

## Optical Response of a New Type of Pyrochlore Oxides $\text{Sm}_2\text{Mo}_2\text{O}_7$ and $\text{Pb}_2\text{Ir}_{2-x}\text{O}_7$

M. Nishiyama<sup>1</sup>, K. Shoji<sup>1</sup>, A. Irisawa<sup>1</sup>, T. Nanba<sup>1</sup>, K. Miyoshi<sup>2</sup> and K. Matsuhira<sup>3</sup>

<sup>1</sup>Kobe University, Nada-ku, Kobe 657-8501, Japan

<sup>2</sup>Shimane University, Matsue 690-8504, Japan

<sup>3</sup>Kyushu Institute of Technology, Tsukuba 305-0047, Japan

### Introduction

$\text{Sm}_2\text{Mo}_2\text{O}_7$  and  $\text{Pb}_2\text{Ir}_{2-x}\text{O}_7$  are well known as typical pyrochlore oxides and have been recently synthesized. These oxide compounds crystallize in a so-called pyrochlore-type structure in which rare earth and transition metal element form respectively 3-dimensional network and Ir element locates at the central position of the tetragon of oxygen atoms. The recent electrical resistivity experiment revealed that at atmospheric pressure, both specimens exhibit a metallic property but their magnetic properties have attracted significant attention due to the geometrical frustration inherent in its crystal structure. That is,  $\text{Sm}_2\text{Mo}_2\text{O}_7$  exhibits paramagnetic states to a spin-glass state at low temperature. On the other hand,  $\text{Pb}_2\text{Ir}_{2-x}\text{O}_7$  which contains nonmagnetic element instead of rare earth element is considered to be a good a reference material. To study its fundamental electronic states close to the Fermi level at ambient pressure, we measured the temperature dependence of optical reflectivity spectra  $R(\omega)$  of  $\text{Sm}_2\text{Mo}_2\text{O}_7$  and  $\text{Pb}_2\text{Ir}_{2-x}\text{O}_7$ .

### Experimental

The optical reflectivity spectra  $R$  at ambient pressure were measured in the wide photon energy range from 7 meV to 30 eV in the temperature range of 8-300 K. The measurements were performed using a Fourier-transform interferometer combined with a thermal light source and synchrotron radiation source at the beam line BL6B & 7B of UVSOR. The optical conductivity  $\sigma_1(\omega)$  and complex dielectric function  $\epsilon_1(\omega)$  were obtained from a standard Kramers-Kronig (K-K) transformation of the measured reflectivity ( $R$ ) spectrum.

### Results and discussions

Figure 1 shows the temperature dependence of the  $R$ -spectra of  $\text{Sm}_2\text{Mo}_2\text{O}_7$ . The spectra in the low energy region exhibit a strong Drude component due to the free conduction electrons which grows with cooling. The peaks at 2.6, 8.0 and 20 eV from a visible to vacuum ultraviolet originate to the electronic interband transition.

Figure 2 shows the temperature dependence of the  $R$ -spectra of  $\text{Pb}_2\text{Ir}_{2-x}\text{O}_7$ . The spectra at room temperature exhibit a metallic property, but with decreasing of temperature, the overall spectra change to insulating properties. Particularly, in the low energy part of the  $R$ -spectra around 0.08-0.8 eV, a distinct decrease in the reflectivity. This clear

appearance of the structure means the occurrence of the stabilization of the insulating phase which induces the formation of the energy gap. The analysis is now on progress.

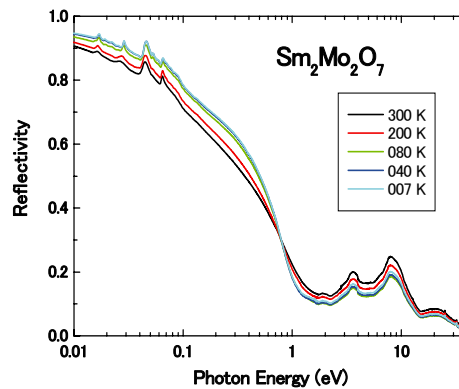


Fig. 1. Temperature dependence of  $R$ -spectra of  $\text{Sm}_2\text{Mo}_2\text{O}_7$ . Note to the abscissa in logarithmic scale.

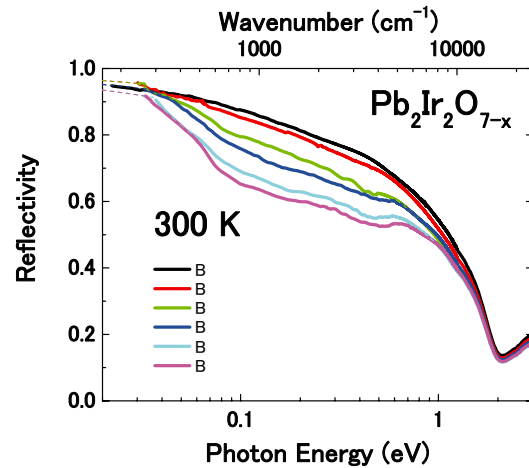


Fig. 2. Temperature dependence of  $R$ -spectra of  $\text{Pb}_2\text{Ir}_{2-x}\text{O}_7$ . Note to the abscissa in logarithmic scale.

[1] K. Miyoshi *et al.*, J. Phys. Jpn. **75** (2006) 065001-1.

## Angle-Resolved Photoemission Study on $\text{EuFe}_2\text{As}_2$

T. Ito<sup>1,2</sup>, J. B. Hong<sup>3</sup>, Y. R. Jang<sup>3</sup>, S. Kimura<sup>1,2</sup> and Y. S. Kwon<sup>3</sup>

<sup>1</sup>*UVSOR Facility, Institute for Molecular Science, Okazaki 444-8585, Japan*

<sup>2</sup>*School of Physical Sciences, the Graduate University for Advanced Studies (SOKENDAI), Okazaki 444-8585, Japan*

<sup>3</sup>*Department of Physics, Sungkyunkwan University, Suwon 440-749, Korea*

Recent discovery of a new high-temperature ( $T_c$ ) superconductor, iron (Fe) pnictides, has triggered intensive researches, since the foregoing common sense that the magnetism must be the obstacle for superconductivity has been disproved [1]. Since the compounds commonly exhibit a collinear antiferromagnetic (AF) spin density wave (SDW), which can be connected to the pseudo-gap phase of cuprate high- $T_c$  superconductors [2], the relation between SDW and superconductivity becomes a new topic on strongly-correlated electron systems.

$\text{EuFe}_2\text{As}_2$ , which exhibits a SDW transition around  $T_0=190$  K at  $\text{Fe}_2\text{As}_2$  layer, shows the antiferromagnetic ordering at  $T_N = 20$  K of the localized  $\text{Eu}^{2+}$  moments [3]. With applying pressure, the SDW temperature decreases in spite of the constant  $T_N$ . Furthermore, superconductivity  $T_c = 30$  K appears under high pressure or due to the K doping [4]. Thus  $\text{EuFe}_2\text{As}_2$  is an ideal system to study the essential role of the SDW formation to the mechanism of high- $T_c$  superconductivity.

Figure 2(b) shows the band structure near  $E_F$  of  $\text{EuFe}_2\text{As}_2$  at the SDW phase ( $T = 25$  K). From the comparison with the results of  $\text{Ba}_{0.6}\text{K}_{0.4}\text{Fe}_2\text{As}_2$ , observed Fermi surfaces (FSs) (see Figs. 1 and 2(a)) are attributed to a tetragonal shaped hole-like FS ( $\beta$ ) around the  $\Gamma$  point and an ellipsoidal shaped electron-like one ( $\gamma$ ) around the M point. When we focus on to the hole-pocket, we found a faint dispersive feature that can be attributed to the folded band originating from the electron-pocket at the M point shifted by an antiferromagnetic SDW vector. It should be noted that the SDW formation has been expected between the electron-like FS ( $\gamma$ ) at the M point and the smaller hole-like FS ( $\alpha$ ) at the  $\Gamma$  point in  $\text{Ba}_{0.6}\text{K}_{0.4}\text{Fe}_2\text{As}_2$  system [1], though the latter seems to be fully occupied at the present  $\text{EuFe}_2\text{As}_2$  case. To further insight into the essential role of the observed SDW feature, its temperature dependence across SDW transition temperature as well as  $T_N$ , and the doping dependence are intended.

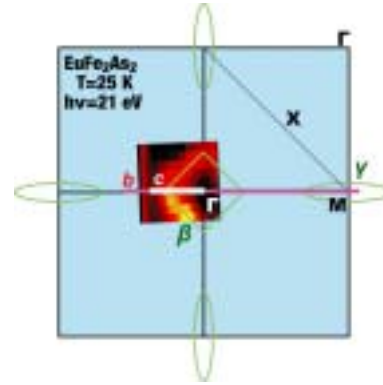


Fig. 1. Fermi surface image of  $\text{EuFe}_2\text{As}_2$  compared with the expected Fermi surface topology from the previous report on  $\text{Ba}_{0.6}\text{K}_{0.4}\text{Fe}_2\text{As}_2$  [1].

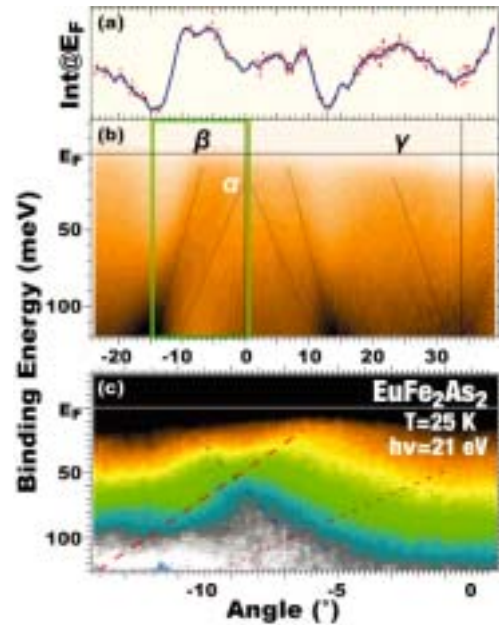


Fig. 2. (a) Angular distribution curve at  $E_F$  and (b) band structure near  $E_F$  of  $\text{EuFe}_2\text{As}_2$  at the SDW phase ( $T = 25$  K). (c) Band structure near  $E_F$  enlarged around the hole-pocket ( $\beta$ ). Dashed lines are guide for eyes.

- [1] H. Ding *et al.*, *Eur. Phys. Lett.* **83** (2008) 47001.  
 [2] S. V. Borisenko *et al.*, *Phys. Rev. Lett.* **100** (2008) 196402.  
 [3] H. S. Jeevan *et al.*, *Phys. Rev. B* **78** (2008) 020503(R).  
 [4] H. S. Jeevan *et al.*, *Phys. Rev. B* **78** (2008) 092406.

## High-Resolution Angle-Resolved Photoemission Study of High- $T_c$ Cuprate Superconductors: Observation of Bulk Electronic States

K. Nakayama<sup>1</sup>, T. Arakane<sup>1</sup>, S. Souma<sup>2</sup>, K. Terashima<sup>3</sup>, T. Sato<sup>1</sup> and T. Takahashi<sup>1,2</sup>

<sup>1</sup>Department of Physics, Tohoku University, Sendai 980-8578, Japan

<sup>2</sup>WPI Research Center, Advanced Institute for Material Research, Tohoku University, Sendai 980-8577, Japan

<sup>3</sup>UVSOR Facility, Institute for Molecular Science, Okazaki 444-8585, Japan

Low-energy excitations play an essential role in characterizing various physical properties such as superconductivity and the metal-insulator transition. In copper-oxide (cuprate) high- $T_c$  superconductors (HTSC), low-energy excitations are intensively studied by the high-resolution angle-resolved photoemission spectroscopy (ARPES). Numerous amounts of ARPES researches have been focused on a bilayered Bi-based HTSC  $\text{Bi}_2\text{Sr}_2\text{CaCu}_2\text{O}_8$  (Bi2212), because of its high  $T_c$  value and good surface condition suitable for ARPES. Previous ARPES studies of Bi2212 clarified several characteristic features essential to the high- $T_c$  superconductivity, such as the large Fermi surface centered at the  $(\pi, \pi)$  point of the Brillouin zone, the  $d_{x^2-y^2}$ -wave superconducting gap, the emergence of well-defined Bogoliubov quasiparticles below  $T_c$  in antinodal region, and the pseudogap above  $T_c$  in an underdoped regime. However, it is still unclear whether or not these characteristic low-energy excitations are generic feature of all HTSCs. Hence the universality of essential character of  $\text{CuO}_2$  plane should be examined by performing ARPES of other families of HTSCs. In this regard,  $\text{YBa}_2\text{Cu}_3\text{O}_{7-\delta}$  (Y123) is most suitable candidate since it is also a bilayered system with similar maximum  $T_c$ , and the bosonic excitations are intensively studied by other experiments. However, it is well known from the earlier stage of ARPES investigations on Y-based HTSCs that the electronic structure is fairly complicated owing to the experimental facts that the superconducting gap is not as robust as that of Bi2212 and is not clearly observed even below  $T_c$ , and strong emission from the surface-state in the antinodal region dominates the low-energy excitations, causing a difficulty in distinguishing bulk electronic signal from the  $\text{CuO}_2$  plane.

In this study, we overcome these difficulties by utilizing the low-energy and variable polarization characters of the beamline BL-7U, and we have succeeded in directly observing the signature of bulk superconducting gap in Y123.

Figure 1(a) shows the ARPES spectral intensity plot of Y123 ( $T_c = 92$  K) at  $E_F$  measured at 15 K with 24.5-eV photons using a linearly polarized light whose polarization direction is shown in (a). ARPES intensity at  $E_F$  is obtained by integrating the intensity within 10 meV with respect  $E_F$ . We clearly

identify large hole-like Fermi surfaces centered at the  $(\pi, \pi)$  point of the Brillouin zone, consistent with the previous ARPES study with higher energy photons [1]. These features mainly originate in the surface-derived bonding and antibonding bands. In order to see dispersive feature of energy bands, we have measured energy distribution curves along a cut shown by a blue line in (a). The result is illustrated in Fig. 1(b). We clearly observed a highly dispersive band which apparently crosses  $E_F$ . This band is attributed to the surface band, since it is metallic even below bulk  $T_c$ . Moreover, as indicated by markers, we find less dispersive feature at  $\sim 30$  meV which does not cross  $E_F$ . This band is assigned as a bulk band showing a superconducting gap of 30 meV in the antinodal region. We thus conclude from the present experimental result that bulk electronic structure of Y123 can be clearly resolved when we optimize the photon energy and the polarization vector of incident light.

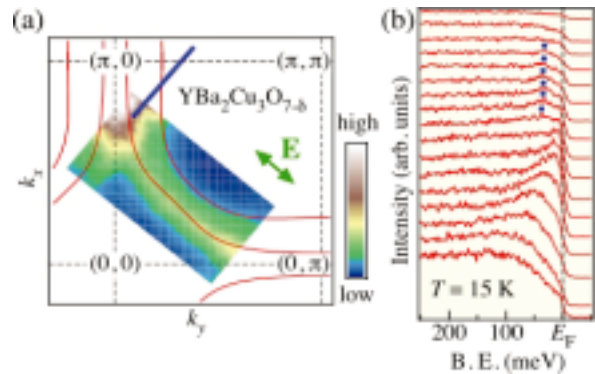


Fig. 1. (a) ARPES intensity of Y123 measured at 15 K with  $h\nu = 24.5$  eV plotted as a function of in-plane wave vector, together with the tight-binding fitting result of the surface band (solid curves). Polarization direction of light is indicated in the inset. (b) Energy distribution curves measured along the cut indicated by a blue line in (a).

[1] K. Nakayama *et al.*, Phys. Rev. B **75** (2007) 014513.

## Extremely Low-Energy Photoemission Study of $\text{Sm}_{1-x}\text{Eu}_x\text{B}_6$

A. Sekiyama<sup>1</sup>, J. Yamaguchi<sup>1</sup>, S. Komori<sup>1</sup>, H. Sugiyama<sup>1</sup>, M. Y. Kimura<sup>1</sup>, S. Ye<sup>2</sup>, S. Lee<sup>3</sup>,  
H. Kim<sup>4</sup>, T. Ito<sup>5</sup>, S. Kimura<sup>5</sup> and S. Suga<sup>1</sup>

<sup>1</sup>Graduate School of Engineering Science, Osaka University, Toyonaka, Osaka 560-8531, Japan

<sup>2</sup>Korea Atomic Energy Research Institute, Daejeon 305-600, Korea

<sup>3</sup>Department of Physics, Sogang University, Seoul 121-742, Korea

<sup>4</sup>Pohang Accelerator Laboratory, Pohang 790-784, Korea

<sup>5</sup>UVSOR Facility, Institute for Molecular Science, Okazaki 444-8585, Japan

$\text{SmB}_6$  and  $\text{YbB}_{12}$  are known as Kondo semiconductors showing a nonmagnetic semiconducting behavior at low temperatures. It is thought that this nature originates from the formation of the hybridization gap in the vicinity of the Fermi level ( $E_F$ ), which reflects the periodicity of the 4f sites. Recently, we have found the collapse of the 4f lattice coherence is collapsed for a partially Lu-substituted system  $\text{Yb}_{1-x}\text{Lu}_x\text{B}_{12}$  by temperature-dependent hard x-ray photoemission (HAXPES), suggesting that the hybridization gap is no longer opened for  $x = 0.125$  due to the lack of the 4f periodicity [1]. On the other hand, it is also found that the temperature dependence of the 4f HAXPES spectra for  $\text{Sm}_{0.85}\text{Eu}_{0.15}\text{B}_6$  ( $x = 0.15$ ) is qualitatively similar to that for pure  $\text{YbB}_{12}$  while the bulk spectra of  $\text{Sm}_{0.5}\text{Eu}_{0.5}\text{B}_6$  ( $x = 0.5$ ) could be explained by the single impurity Anderson model without considering the 4f periodicity. These results imply that the hybridization gap is still present for the Eu-substituted system  $\text{Sm}_{0.85}\text{Eu}_{0.15}\text{B}_6$ . In order to directly verify the presence of the gap, we have performed the extremely low-energy photoemission (ELEPES) study for  $\text{Sm}_{1-x}\text{Eu}_x\text{B}_6$ .

ELEPES was performed at BL7U by using a photoelectron spectrometer of MB Scientific A1 analyzer. In order to obtain clean surfaces, the bulk  $\text{Sm}_{1-x}\text{Eu}_x\text{B}_6$  samples were fractured *in situ* at 15 K. We measured the photoemission spectra by controlling  $h\nu$  from 7 to 17 eV. The energy resolution was set to  $<10$  meV at  $h\nu = 7$  eV. We checked the reproducibility of the temperature dependence of the spectra for  $\text{Sm}_{0.85}\text{Eu}_{0.15}\text{B}_6$  by measuring the spectra on heating from 15 to 200 K and those on cooling from 200 to 15 K for the same sample without any surface treatment after fracturing at 15 K.

Figure 1 shows the  $h\nu$  dependence of the valence-band spectra near  $E_F$  for  $\text{Sm}_{0.85}\text{Eu}_{0.15}\text{B}_6$ . A narrow peak located at about 15 meV is seen in the spectra at  $h\nu = 7, 8.4$  and  $9.7$  eV. This peak is strongly smeared in the spectra at  $h\nu = 12$  and  $14$  eV, and seems to disappear in the spectrum at  $h\nu = 17$  eV. The spectral weight in the vicinity of  $E_F$  seems to increase slightly but gradually with  $h\nu$ . Considering that the spectral line shape does not change among the spectra at  $h\nu = 7, 8.4$  and  $9.7$  eV, we conclude that the narrow peak at  $\sim 15$  meV reflects the bulk band

structure at low temperatures, and that ELEPES is surely bulk-sensitive at  $h\nu < 10$  eV. The leading-edge, the binding energy at which the spectral intensity is half of that at the peak or shoulder nearest to  $E_F$ , is apparently in the occupied side in the spectra at  $h\nu < 10$  eV, which indicates that the finite gap is open even for the Eu-substituted system  $\text{Sm}_{0.85}\text{Eu}_{0.15}\text{B}_6$ .

The temperature-dependent spectra of  $x = 0.15$  at  $h\nu = 7$  eV (not shown here) indicate that the spectral weight in the vicinity of  $E_F$  is gradually enhanced with temperature up to 200 K, suggesting that the gap is closed at high temperatures. On the other hand, such a temperature dependence is not seen for  $x = 0.5$ , which gives a metallic Fermi cut-off in the spectra at 15 and 200 K. This result reflects that the hybridization gap as well as the 4f lattice coherence collapses even at low temperatures for the “heavily” substituted  $x = 0.5$ . From these results, we would conclude that  $\text{SmB}_6$  is a “robust” Kondo semiconductor against a rare-earth substitution, which is in strong contrast to the case for  $\text{YbB}_{12}$ .

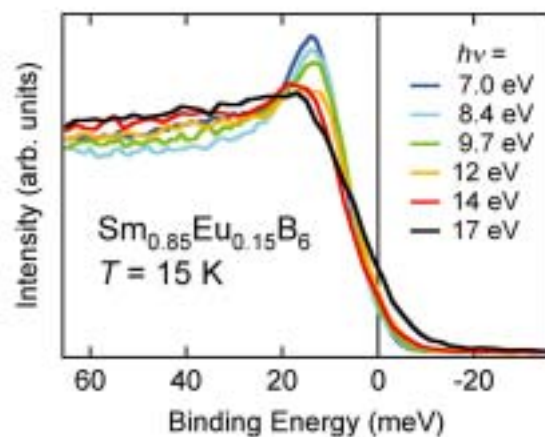


Fig. 1.  $h\nu$  dependence of the valence-band photoemission spectra near  $E_F$  for  $\text{Sm}_{0.85}\text{Eu}_{0.15}\text{B}_6$ .

[1] J. Yamaguchi *et al.*, Phys. Rev. B, in press.

[2] J. Yamaguchi *et al.*, unpublished.

## Anisotropic Electron-Scattering and Thermoelectric Power of $\text{La}_{2-x}\text{Sr}_x\text{CuO}_4$ and $\text{Nd}_{2-x}\text{Sr}_x\text{CuO}_4$ Superconductors

T. Takeuchi<sup>1, 2</sup>, H. Komoto<sup>2</sup>, Y. Hamaya<sup>2</sup>, S. Arita<sup>2</sup>, T. Ito<sup>3</sup> and S. Kimura<sup>3</sup>

<sup>1</sup>*EcoTopia Science Institute, Nagoya University, Nagoya 464-8603, Japan*

<sup>2</sup>*Department of Crystalline Materials Science, Nagoya University, Nagoya 464-8603, Japan*

<sup>3</sup>*UVSOR Facility, Institute for Molecular Science, Okazaki 444-8585, Japan*

After the prediction of the potential of low-dimensional systems as a practical thermoelectric material [1, 2], a considerable attention has been attracted in the materials with low dimensional crystal structure. High- $T_c$  superconductors, such as  $\text{La}_{2-x}\text{Sr}_x\text{CuO}_4$  (LSCO) and  $\text{Nd}_{2-x}\text{Sr}_x\text{CuO}_4$  (NCCO), are typical materials possessing two-dimensional atomic and electronic structures. Notably, LSCO and NCCO with small  $x$  possess a large thermoelectric power exceeding 100  $\mu\text{V}/\text{K}$  and metallic electrical conduction.

Although important role of two-dimensional electronic structure was predicted from the theoretical considerations [1, 2], the relation between the theory and the good thermoelectric properties of LSCO and NCCO has not been clearly understood yet. The small magnitude of thermoelectric power observed for  $\text{Bi}_2\text{Sr}_2\text{CuO}_{6+\delta}$  possessing an electronic structure similar to that of LSCO and NCCO might indicate less important role of two-dimensional electronic structure. It is, therefore, of great importance to study the origin of the characteristic thermoelectric properties observed for LSCO and NCCO.

LSCO possess positive sign in its thermoelectric power over a wide temperature range while NCCO negative one. This fact seemingly sounds natural because LSCO and NCCO are obtained by doping some holes or electrons in the Mott insulator, respectively, and the Mott insulator has the fully occupied lower Hubbard-band and upper Hubbard-band separated from each other by an energy gap. These Hubbard-bands, however, are known to disappear in LSCO and NCCO and to be replaced by a single band crossing the Fermi level. This experimentally revealed fact definitely indicates that the sign and magnitude of thermoelectric power of LSCO and NCCO cannot be simply accounted for with the Mott-Hubbard bands.

In this study, therefore, we investigated the energy-momentum dispersion and the lifetime of the coherent states (Bloch states or quasiparticles) in LSCO and NCCO using the high-resolution angle resolved photoemission spectroscopy (APRES) measurements. By using the obtained information about the electric states, we calculated thermoelectric power by using the semi-classical Boltzmann equation and compared it with the measured data.

By accumulating ARPES data over the whole momentum space, we realized that the

energy-momentum dispersion of these two compounds looks very similar to each other except for the clear difference in the Fermi level, and that the electron scattering exhibits strong anisotropy, which is characterized by the “hot spot” and “cold spot”, in both compounds. We also realized by analyzing the spectral shape at each Fermi momentum that the “hot spot”, where the quasiparticles are most frequently scattered, is located near  $(\pi, \pi)$  in LSCO, while it stays at the momentum near  $(\pi/2, \pi/2)$  in NCCO. This fact is naturally understood by assuming that the “hot spot” is created by the fluctuation of anti-ferromagnetic ordering and hence it is located at the momentum where the Fermi surface (FS) crosses the anti-ferromagnetic zone boundary (AFZB). Indeed the large holelike Fermi surface in LSCO intersects AFZB near  $(\pi, \pi)$  while the small holelike FS in NCCO near  $(\pi/2, \pi/2)$ .

We calculated thermoelectric power with considering the strong scattering effect at the AFZB. The calculated thermoelectric power is shown in Fig. 1 together with the measured data. Obviously, the calculation quantitatively reproduced the measured data at least in the temperature range we used in the calculation. We also calculated thermoelectric power without the effect of strong scattering at the AFZB, and found that the large magnitude nor the sign of thermoelectric power are unable to be reproduced without the AFZB-effect. We conclude, therefore, that the large magnitude of the thermoelectric power is caused by the anisotropic electron-scatterings while the two-dimensionality has less important role on it.

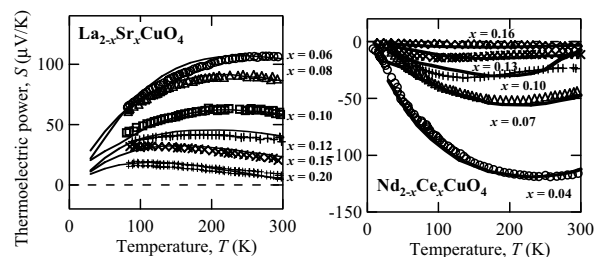


Fig. 1. The calculated and measured thermoelectric power of  $\text{La}_{2-x}\text{Sr}_x\text{CuO}_4$  and  $\text{Nd}_{2-x}\text{Ce}_x\text{CuO}_4$ .

[1] L. D. Hicks and M. S. Dresselhaus, Phys. Rev. B **47** (1993) 12727.

[2] L. D. Hicks and M. S. Dresselhaus, Phys. Rev. B **47** (1993) 16631.

## Valence Band Structure Study of AlN

T. Ito<sup>1</sup>, R. Ikematsu<sup>1</sup>, M. Kishida<sup>1</sup>, K. Fukui<sup>1</sup>, K. Hiramatsu<sup>2</sup>, H. Amano<sup>2</sup> and H. Hirayama<sup>3</sup>

<sup>1</sup>Department of Electrical and Electronics Engineering, University of Fukui, Fukui 910-8507, Japan

<sup>2</sup>Department of Material Science Engineering, Meijo University, Aichi 468-8507, Japan

<sup>3</sup>RIKEN, Saitama 351-0198, Japan

Aluminum nitride (AlN) has the widest direct band-gap in III-V nitride compound semiconductors, so that AlN is expected such applications as UV light emitting diodes, *etc.* It is known that the uppermost valence band (VB) of AlN splits into three levels (CH, HH and LH bands in increasing band-gap order) due to crystal-field splitting and spin orbit interaction, and transition between each level and conduction band (CB) has the different polarization character. These three transitions are usually labeled as A (from CH to CB), B (HH to CB), and C (LH to CB). B and C transitions are mainly allowed under  $E \perp c$  condition, while A transition is only allowed under  $E \parallel c$  condition, where  $E$  and  $c$  represent the electric field vector of the excited light and the crystal axis of wurtzite AlN, respectively. It means that the transition at the minimum band-gap (A transition) becomes forbidden, because  $c$ -axes of AlN thin films grown on both sapphire and SiC substrates are usually perpendicular to the surface. Then, an understanding of the VB structure is necessary not only for basic science but also for application. Therefore, optical reflectance (OR) spectra, photoluminescence (PL), and PL excitation (PLE) spectra measurements at low temperature have been performed to observe all transitions near band edge (including A to C transitions and estimation of both the crystal-field splitting energy  $\Delta_{cr}$  and spin-orbital splitting energy  $\Delta_{so}$ ) and their polarization characters. To measure all transitions including forbidden transitions under normal incidence light configuration, OR and PLE spectra measurements have been carried out with rotating incident light angle under  $p$  optical configuration using highly linear polarized synchrotron radiation excitation light.

AlN films were grown on the sapphire substrates by MOCVD method. Thicknesses are 1 ~ 3.5  $\mu\text{m}$  for avoiding the stress by the lattice constant mismatch with the substrate. The rotation angle of the incident light is defined as the angle between excitation light and normal vector of sample surface ( $c$  axis).

Figure 1 shows OR spectra at 20 K. OR spectrum at 60 degree clearly shows the structure due to the excitonic absorption around 6.05 eV. It shows that the transition energy of A transition is 6.05 eV, because this structure has clear incident light angle dependence and increases its intensity under  $E \parallel c$  configuration. Adjacent two excitonic structures due to B and C transitions around 6.1 ~ 6.4 eV are

analyzed by the line shape fitting using the theoretical function of exciton absorption [1], and B and C transitions are located at 6.24 and 6.28 eV, respectively. Therefore, based on theoretical model [3],  $\Delta_{cr}$  and  $\Delta_{so}$  are -205 meV and 55 meV, respectively. Figure 2 shows PLE spectra and inset figure shows PL spectrum at 20 K. PL spectrum does not show the incidence light angle dependence. PL peak at 6.05 eV is the main peak and two small peaks at low energy side are LO replicas. Integrated intensities of main PL peaks at 0 and 60 degrees as the function of the excitation photon energy are plotted as PLE spectra. Two peaks which correspond to B and C transitions and two other peaks above 6.4 eV are clearly observed. They are all excited both  $E \perp c$  and  $E \parallel c$  conditions. However, significant difference is shown below 6.24 eV (B transition).

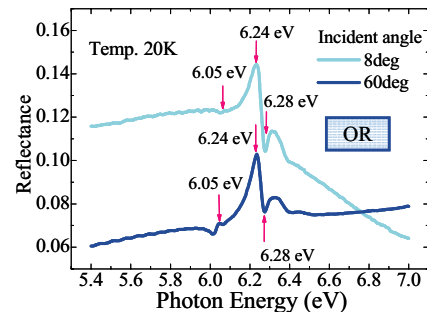


Fig. 1. Incident angle dependence of OR spectra

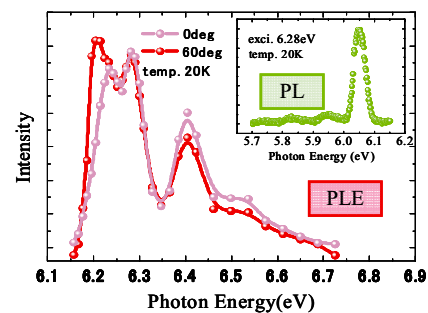


Fig. 2. Incident angle dependence of PLE spectra with PL spectrum (inset).

[1] T. Onuma, S. F. Chichibu, T. Sota, K. Asai, S. Sumiya, T. Shibata and M. Tanaka, *Appl. Phys. Lett.* **81** (2002) 652.

[2] A. Sedhain, J. Y. Lin and H. X. Jiang, *Appl. Phys. Lett.* **92** (2008) 041114.

## Electronic Structures of YbS and Yb Studied by Optical and Photoemission Spectroscopies

H. Okamura<sup>1</sup>, M. Matsunami<sup>2</sup>, T. Nanba<sup>1</sup> and A. Ochiai<sup>3</sup>

<sup>1</sup>Graduate School of Science, Kobe University, Kobe 657-8501, Japan

<sup>2</sup>Institute for Solid State Physics, University of Tokyo, Kashiwa, Chiba 277-8581, Japan

<sup>3</sup>Center for Low Temperature Science, Tohoku University, Aoba-ku, Sendai 980-8578, Japan

In the field of strongly correlated  $f$  electron physics, it is often important to estimate the average valence of rare earth element such as Ce and Yb, since the average valence is directly related to the degree of  $f$  electron localization and delocalization. Such a localization/delocalization duality is believed to be closely related with interesting phenomena such as heavy fermion formation and magnetic quantum criticality. Along with the thermodynamic techniques such as magnetic susceptibility, spectroscopic techniques such as X-ray absorption (XAS) and photoemission (PES) spectroscopies have been very useful in estimating the average valence of a Ce or Yb compound. However, these spectroscopic techniques have sometimes yielded an average valence inconsistent with that given by the thermodynamic properties. For example, YbS and Yb metal are both believed to be divalent compounds from their thermodynamic properties and general considerations on their electronic structures, yet some XAS and PES results have suggested that they are in mixed-valent states [1-3]. In the case of PES, the estimation of average valence usually involves a comparison of spectral weight between the  $\text{Yb}^{2+}$  and  $\text{Yb}^{3+}$  components. It is sometimes difficult to distinguish between a  $\text{Yb}^{3+}$  component and a satellite associated with the  $\text{Yb}^{2+}$  component, which may have resulted in the inconsistent results.

To resolve this question, we have measured X-ray PES spectra of YbS and Yb at SPring-8, and have compared the results with their optical spectra measured at BL7B of UVSOR [4]. Regarding the optical spectra, the reflectivity  $R(\omega)$  of YbS and Yb was measured at BL7B, and their complex dielectric function  $\epsilon$  was obtained from the Kramers-Kronig analysis of  $R(\omega)$ . Then the bulk and surface energy loss functions were calculated as  $\text{Im}(1/\epsilon)$  and  $\text{Im}[1/(\epsilon+1)]$ , respectively. Figure 1 shows the measured Yb 3d core-level PES of YbS (a) and Yb (b), measured with incident photon energy of 7.94 keV at SPring-8, and the energy loss functions obtained at BL7B as described above. The sharp peak near 1520 eV is the  $\text{Yb}^{2+}$  main peak. For the more bulk-sensitive,  $\theta=0$  (normal incidence) spectrum, the satellite located to the left of the main peak has fine structures that correspond to peaks in the bulk loss function very well. In contrast, the more surface-sensitive,  $\theta=80^\circ$  (grazing incidence)

spectrum has a satellite that corresponds to the surface loss function very well. Based on this set of data and the valence band PES spectra measured with soft X-ray incident light, it is concluded that the  $\text{Yb}^{3+}$  component in YbS and Yb is negligibly weak, and these compounds are in fact purely divalent in terms of spectroscopic point of view. Namely, the  $f$  electrons in YbS and Yb are completely localized and forming a closed 4f shell.

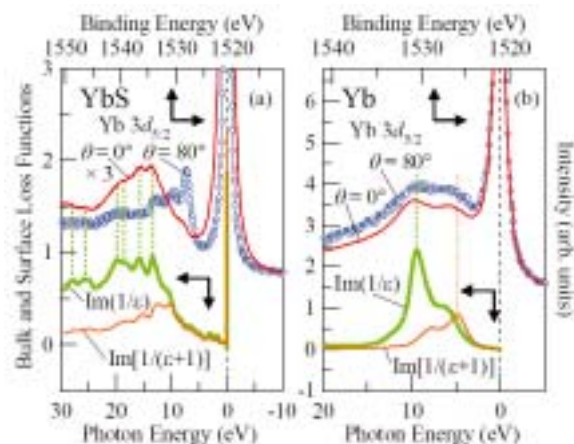


Fig. 1. Yb 3d<sub>5/2</sub> core-level PES spectra of YbS (a) and Yb metal (b), measured at SPring-8, and the bulk and surface loss functions  $\text{Im}(1/\epsilon)$  and  $\text{Im}[1/(\epsilon+1)]$ , respectively, measured at BL7B of UVSOR [4].

- [1] E. Annese, J. P. Rueff, G. Vanko, M. Grioni, L. Braicovich, L. Degiorgi, R. Gusmeroli and C. Dallera, *Phys. Rev. B* **70** (2004) 075117.
- [2] A. Fuse, G. Nakamoto, M. Kurisu, N. Ishimatsu and H. Tanida, *J. Alloys Compounds* **376** (2004) 34.
- [3] C. Dallera, O. Wessely, M. Colarieti-Tosti and O. Eriksson, *Phys. Rev. B* **74** (2006) 081101.
- [4] M. Matsunami, A. Chainani, M. Taguchi, R. Eguchi, Y. Ishida, Y. Takata, H. Okamura, T. Nanba, M. Yabashi, K. Tamasaku, Y. Nishino, T. Ishikawa, Y. Senba, H. Ohashi, N. Tsujii, A. Ochiai and S. Shin, *Phys. Rev. B* **78** (2008) 195118.

## Near Band Edge Photoluminescence and Photoluminescence Excitation Spectra of Mg-Doped $\text{Al}_x\text{Ga}_{1-x}\text{N}$

M. Suzuki<sup>1</sup>, S. Sawai<sup>1</sup>, K. Fukui<sup>1</sup>, K. Nagamatsu<sup>2</sup> and H. Amano<sup>2</sup>

<sup>1</sup> Department of Electrical and Electronics Engineering, University of Fukui, Fukui 910-8507, Japan

<sup>2</sup> Department of Material Science Engineering, Meijo University, Nagoya 468-8502, Japan

The undoped AlGa<sub>N</sub> alloys always show the n-type conduction due to the Nitrogen defects. Then, p-type AlGa<sub>N</sub> alloys are expected to achieve electronic devices, and Mg has been used for the typical dopant. However, it seems that the optical investigations of Mg doped AlGa<sub>N</sub> (AlGa<sub>N</sub>:Mg) are mainly concentrated to the Mg related broad emission band (Mg-related band) which is located between near band edge (NBE) emission band and impurity related broad emission band (so-called Yellow emission). However, NBE emission is also affected by Mg doping. Then, in this study, we investigate the Mg doping effects by the NBE photoluminescence (PL) and PL excitation (PLE) spectra of  $\text{Al}_x\text{Ga}_{1-x}\text{N}$ :Mg in the wide  $x$  range, though we observe both Mg-related band and impurity related broad emission band.

The wurtzite AlGa<sub>N</sub>:Mg films of 1.5  $\mu\text{m}$  thickness are grown on the c-plane sapphire substrates covered with 2  $\mu\text{m}$  thickness highly crystalline AlN layers by MOVPE [1]. The measurement temperature is from 10 to 160 K.

Figure 1 shows the PL and PLE peak energies of four AlGa<sub>N</sub>:Mg samples as a function of Al fraction at 10 K. Two curves represent calculated PL and PLE peaks of undoped AlGa<sub>N</sub>. The peaks of AlGa<sub>N</sub>:Mg are in agreement with those of AlGa<sub>N</sub>. Figure 2 shows the temperature dependence of NBE emission peak energy shifts of  $\text{Al}_{0.65}\text{Ga}_{0.35}\text{N}$ :Mg. Temperature dependence of the peak energy shows S-shaped (decrease – increase – decrease) behaviour with increasing temperature, which is well observed in that of undoped AlGa<sub>N</sub>. These two results suggest that the mechanism of NBE PL of AlGa<sub>N</sub>:Mg is basically similar to that of undoped AlGa<sub>N</sub>. Figure 3 shows the PL spectrum of  $\text{Al}_{0.65}\text{Ga}_{0.35}\text{N}$ :Mg at 10 K and the fitting result of spectrum deconvolution. This deconvolution is based on the model that NBE PL band of undoped AlGa<sub>N</sub> consists of a main peak and 2 ~ 3 LO phonon replicas, and is in good agreement with experimental results of undoped AlGa<sub>N</sub>. However, an additional (A) band is required in the case of AlGa<sub>N</sub>:Mg. Then, one possibility model is that A band is assigned as the transition to Mg acceptor level. According to this model, activation energies of Mg acceptor which corresponds to the energy difference between PLE peak and A band peak becomes 370 and 320 meV for  $\text{Al}_{0.65}\text{Ga}_{0.35}\text{N}$ :Mg and  $\text{Al}_{0.27}\text{Ga}_{0.73}\text{N}$ :Mg, respectively.

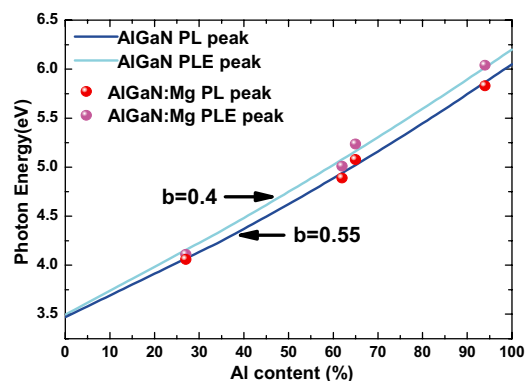


Fig. 1. PL and PLE peaks of AlGa<sub>N</sub>:Mg and undoped AlGa<sub>N</sub> as a function of Al fraction.

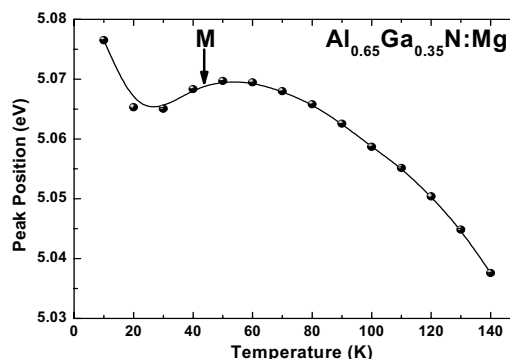


Fig. 2. The temperature dependence of (M) peak energy shifts of  $\text{Al}_{0.65}\text{Ga}_{0.35}\text{N}$ :Mg.

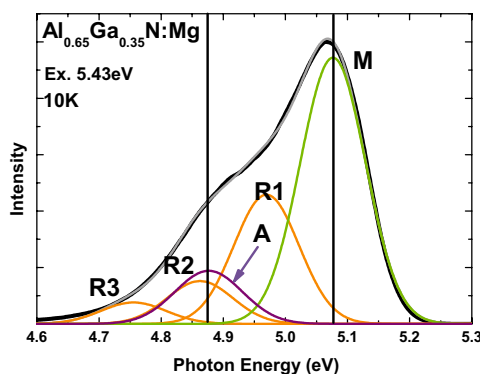


Fig. 3. PL spectrum of  $\text{Al}_{0.65}\text{Ga}_{0.35}\text{N}$ :Mg and fitting result of spectrum deconvolution.

[1] H. Imura, N. Kato, N. Okada, K. Balakrishnan, M. Iwaya, S. Kamiyama, H. Amano, I. Akasaki, T. Noro, T. Takagi and A. Bandoh, Phys. Stat. Sol. **4** (2007) 2502.

## Characterization of Lithium in Minerals by an XAFS Method

T. Kurisaki<sup>1</sup>, Y. Sakogawa<sup>1</sup>, D. Tanaka<sup>1</sup> and H. Wakita<sup>1,2</sup>

<sup>1</sup>*Department of Chemistry, Faculty of Science, Fukuoka University, Jonan-ku, Fukuoka 814-0180, Japan*

<sup>2</sup>*Advanced Materials Institute, Fukuoka University, Jonan-ku, Fukuoka 814-0180, Japan*

Lithium compounds are generally used in industrial and commercial applications such as lithium batteries, lithium glasses and other materials. Sometimes, the lithium is included in minerals, and was tried extract from the minerals. Therefore, it is very interesting to investigate the chemical condition of lithium in minerals. The XAFS method has not been widely used to estimate the electronic structure of lithium in minerals owing to the low energy (below about 70 eV) of Li K edge. However, there are a few reports about Li-K XANES spectra [1,2].

In this work, we applied the X-ray absorption near edge structure (XANES) spectroscopy to lithium in minerals. X-ray absorption spectra of near Li K absorption edges were (XAFS) measured at BL8B1 of the UVSOR in the Institute of Molecular Science, Okazaki [3]. The energy of the UVSOR storage ring was 750 MeV and the stored current was 110-230 mA. The absorption was monitored by the total electron yield using a photomultiplier. We employed the discrete variational (DV)-X $\alpha$  molecular orbital (MO) method to perform calculated spectra, and compared observed spectra with calculated spectra.

The Li K XANES spectra of a lepidolite contained lithium and three reference lithium compounds are shown in Fig. 1. A remarkable change of the spectral patterns was observed for the three reference lithium compounds. But the peak was not observed to a spectrum of the lepidolite. This reason is because lithium ion content in the lepidolite is very small amount (1.5~3%). We are going to try to measured Al K edge XANES of the lepidolite and calculated spectra by DV-X $\alpha$  molecular orbital calculations.

[1] J. Tsuji, K. Kojima, S. Ikeda, H. Nakamatsu, T. Mukoyama and K. Taniguchi, *J. Synchrotron Rad.* **8** (2001) 554.

[2] T. Kurisaki, Y. Nakazono, S. Matsuo, R.C.C. Perera, J. H. Underwood and H. Wakita, *Adv. Quantum Chem.* **54** (2008) 315.

[3] S. Murata, T. Matsukawa, S. Naoè, T. Horigome, O. Matsudo and M. Watanabe, *Rev. Sci. Instrum.* **63** (1992) 1309.

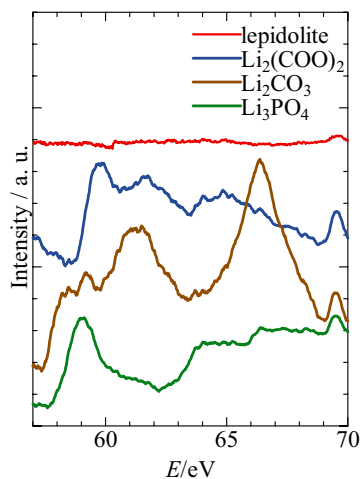


Fig. 1. Li K-edge XANES spectra of a lepidolite and reference lithium compounds.